LETTER

https://doi.org/10.1038/s41586-018-0849-9

Gut intraepithelial T cells calibrate metabolism and accelerate cardiovascular disease

Shun He[1,7]*, Florian Kahles[1,7], Sara Rattik[1,7], Manfred Nairz[1], Cameron S. McAlpine[1], Atsushi Anzai[1], Daniel Selgrade[1], Ashley M. Fenn[1], Christopher T. Chan[1], John E. Mindur[1], Colin Valet[1], Wolfram C. Poller[1], Lennard Halle[1], Noemi Rotllan[2], Yoshiko Iwamoto[1], Gregory R. Wojtkiewicz[1], Ralph Weissleder[1,3,4], Peter Libby[5], Carlos Fernández-Hernando[2], Daniel J. Drucker[6], Matthias Nahrendorf[1,3] & Filip K. Swirski[1,3]*

The biochemical response to food intake must be precisely regulated. Because ingested sugars and fats can feed into many anabolic and catabolic pathways[1], how our bodies handle nutrients depends on strategically positioned metabolic sensors that link the intrinsic nutritional value of a meal with intermediary metabolism. Here we describe a subset of immune cells—integrin β7$^+$ natural gut intraepithelial T lymphocytes (natural IELs)—that is dispersed throughout the enterocyte layer of the small intestine and that modulates systemic metabolism. Integrin β7$^-$ mice that lack natural IELs are metabolically hyperactive and, when fed a high-fat and high-sugar diet, are resistant to obesity, hypercholesterolaemia, hypertension, diabetes and atherosclerosis. Furthermore, we show that protection from cardiovascular disease in the absence of natural IELs depends on the enteroendocrine-derived incretin GLP-1[2], which is normally controlled by IELs through expression of the GLP-1 receptor. In this metabolic control system, IELs modulate enteroendocrine activity by acting as gatekeepers that limit the bioavailability of GLP-1. Although the function of IELs may prove advantageous when food is scarce, present-day overabundance of diets high in fat and sugar renders this metabolic checkpoint detrimental to health.

Although integrin β7 directs immune cells to the gut[3–8], we know little about the influence of this integrin on metabolism, despite the strategic location of the gut as the site where dietary nutrients are absorbed[9]. *Itgb7*$^{-/-}$ (hereafter *β7*$^{-/-}$) mice that were fed a chow diet gained weight in a similar way to control wild-type mice (Fig. 1a), but ate more food (Fig. 1b) despite being equally active (Extended Data Fig. 1a). This inconsistency prompted us to measure energy usage. We found that *β7*$^{-/-}$ mice expended more energy (Fig. 1c) and produced more heat (Fig. 1d), although their respiratory exchange rate was similar to wild-type mice (Extended Data Fig. 1b, c). The data suggest that these mice have a heightened basal metabolism. We therefore performed whole-body ^{18}F-fluorodeoxyglucose ([^{18}F]FDG) and non-invasive, high-resolution positron emission tomography/computed tomography (PET/CT) imaging to assess regional glucose uptake and found that *β7*$^{-/-}$ mice accrued more glucose in the brown fat compared to wild-type controls (Fig. 1e, f and Extended Data Fig. 1d). The *β7*$^{-/-}$ mice were more glucose tolerant (Fig. 1g), even at thermoneutrality (Extended Data Fig. 1e), and had higher levels of plasma insulin (Fig. 1h) without changes in insulin sensitivity (Fig. 1i). The microbiome did not appear to affect these differences (Extended Data Fig. 1f, g). Moreover, the phenomenon was neither restricted to glucose—because *β7*$^{-/-}$ mice had lower levels of fasting triglycerides (Fig. 1j) and better fat tolerance (Fig. 1k) without differences in hepatic secretion of triglycerides (Fig. 1l)—nor associated with fat absorption or gut permeability abnormalities (Extended Data Fig. 1h, i).

We next tested whether the beneficial metabolic alterations in *β7*$^{-/-}$ mice were sustained in the context of the 'metabolic syndrome' component cluster[10]. *β7*$^{-/-}$ mice that were fed a diet high in fat, sugar and sodium (HFSSD) remained relatively lean, in contrast to wild-type controls, which became obese (Fig. 2a). Both inguinal white adipose tissue (iWAT) and perigonadal white adipose tissue (pWAT) were heavier in wild-type mice than in *β7*$^{-/-}$ mice, but other tissue weights remained similar (Fig. 2b). Furthermore, adipocytes in iWAT and pWAT were larger in wild-type mice than in *β7*$^{-/-}$ mice (Fig. 2c–e). Flow cytometry of both iWAT and pWAT showed that fewer Ly-6C^{high} monocytes, neutrophils and macrophages had accumulated in *β7*$^{-/-}$ mice, indicating that *β7*$^{-/-}$ mice were protected from obesity-associated inflammation[11,12] (Extended Data Fig. 2a, b). In contrast to wild-type control mice, *β7*$^{-/-}$ mice did not develop hypertension (Fig. 2f) and—similar to observations made in *β7*$^{-/-}$ mice that were on a chow diet—*β7*$^{-/-}$ mice that were fed a HFSSD remained more glucose-tolerant than wild-type mice (Fig. 2g and Extended Data Fig. 2c, d), indicating that *β7*$^{-/-}$ mice were protected against the adverse metabolic consequences of a high-fat diet.

Because *β7*$^{-/-}$ mice had a higher metabolism and exhibited fewer metabolic syndrome components, we tested whether they had lower rates of atherosclerosis, which is a chronic, lipid-driven inflammatory disease[13]. We generated *Ldlr*$^{-/-}$ chimaeras reconstituted with bone marrow from either *β7*$^{-/-}$ (bm*β7*$^{-/-}$) or wild-type (bm*β7*$^{+/+}$) mice and found that *Ldlr*$^{-/-}$ mice with *β7*$^{-/-}$ bone marrow (bm*β7*$^{-/-}$*Ldlr*$^{-/-}$) that were fed a diet high in cholesterol (HCD) had considerably lower levels of plasma total cholesterol than controls (bm*β7*$^{+/+}$*Ldlr*$^{-/-}$) (Fig. 3a and Extended Data Fig. 2e). The bm*β7*$^{-/-}$*Ldlr*$^{-/-}$ mice had lower levels of very-low-density lipoprotein, intermediate-density lipoprotein and low-density lipoprotein, but similar levels of high-density lipoprotein (Fig. 3b). bm*β7*$^{-/-}$*Ldlr*$^{-/-}$ mice gained weight in a similar manner to bm*β7*$^{+/+}$*Ldlr*$^{-/-}$ controls (Extended Data Fig. 2f), yet tended to excrete more cholesterol (Extended Data Fig. 2g). Moreover, bm*β7*$^{-/-}$*Ldlr*$^{-/-}$ mice had smaller aortic root lesions (Fig. 3c), with a reduction of around 50% in plaque size and volume (Fig. 3d, e). These changes were driven by differences in the size of the necrotic core (Extended Data Fig. 2h–j) and the number of leukocytes (Fig. 3f), the latter of which was independent of β7-mediated recruitment (Extended Data Fig. 3a, b). Because hypercholesterolaemia induces leukocytosis[14], which is a cardiovascular risk factor[15], we also analysed the number of leukocytes in the blood and found fewer circulating Ly-6C^{high} and Ly-6C^{low} monocytes in bm*β7*$^{-/-}$*Ldlr*$^{-/-}$ mice fed a HCD (Fig. 3g), but not in bm*β7*$^{-/-}$*Ldlr*$^{-/-}$ mice fed a chow diet (Extended Data Fig. 3c). Similar to experiments obtained using *β7*$^{-/-}$ mice, we noted improved glucose tolerance in the bm*β7*$^{-/-}$*Ldlr*$^{-/-}$ chimaeras (Extended Data Fig. 3d). We also generated *β7*$^{-/-}$*Ldlr*$^{-/-}$ mice. Following assessment of metabolic functions, which were similar to those in *β7*$^{-/-}$ mice,

[1]Center for Systems Biology, Massachusetts General Hospital and Harvard Medical School, Boston, MA, USA. [2]Vascular Biology and Therapeutics Program, Department of Comparative Medicine and Pathology, Yale University School of Medicine, New Haven, CT, USA. [3]Department of Radiology, Massachusetts General Hospital and Harvard Medical School, Boston, MA, USA. [4]Department of Systems Biology, Harvard Medical School, Boston, MA, USA. [5]Cardiovascular Division, Department of Medicine, Brigham and Women's Hospital, Boston, MA, USA. [6]Mount Sinai Hospital, University of Toronto, Toronto, Ontario, Canada. [7]These authors contributed equally: Shun He, Florian Kahles, Sara Rattik. *e-mail: SHE6@mgh.harvard.edu; fswirski@mgh.harvard.edu

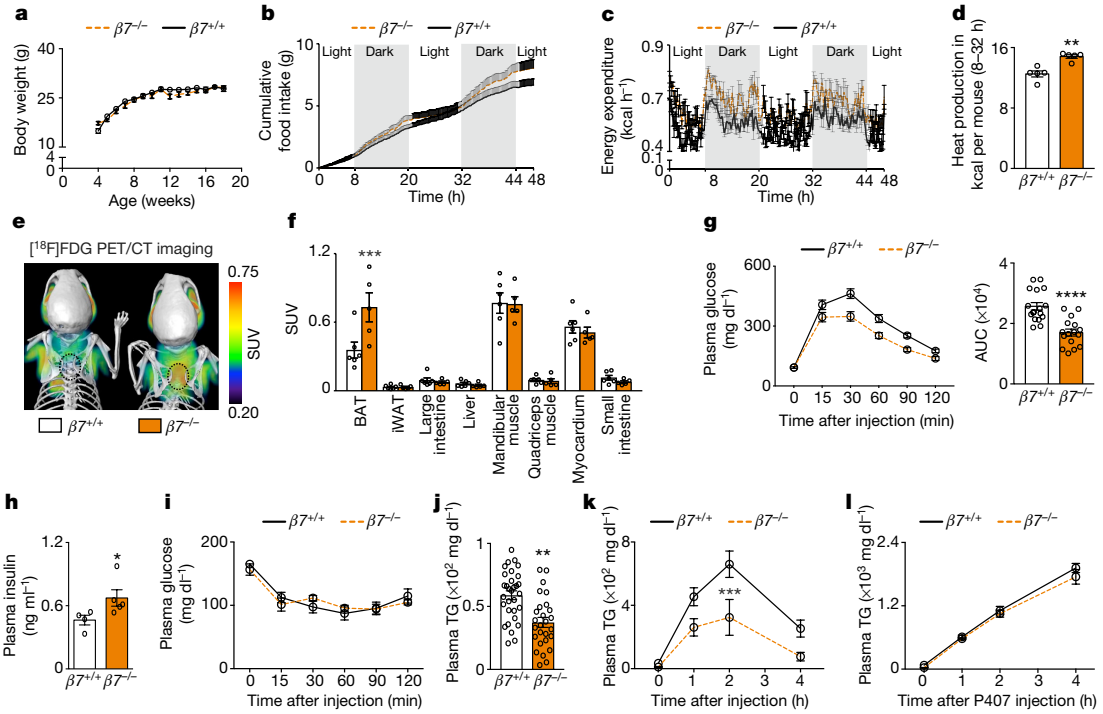

Fig. 1 | Integrin β7 regulates metabolism. a–d, Body weight (**a**), cumulative food intake (**b**), energy expenditure (**c**) and heat production (**d**) in wild-type ($\beta7^{+/+}$) and $\beta7^{-/-}$ mice fed a chow diet. $n = 5$ mice per group. **e**, Representative (of 6 and 5 mice, respectively) PET/CT images after [^{18}F]FDG administration to wild-type and $\beta7^{-/-}$ mice. **f**, Standard update values (SUV) quantified in vivo in indicated regions of interest. $n = 6$ wild-type mice; $n = 5$ $\beta7^{-/-}$ mice. A nonparametric multiple-comparisons test was used. BAT, brown adipose tissue; iWAT, inguinal white adipose tissue. **g**, Left, glucose-tolerance test in wild-type and $\beta7^{-/-}$ mice that were fed a chow diet; after intraperitoneal glucose injection. Right, area under curve (AUC) of intraperitoneal glucose-tolerance test. $n = 17$ wild-type mice; $n = 16$ $\beta7^{-/-}$ mice. **h**, Plasma insulin levels in wild-type and $\beta7^{-/-}$ mice 15 min after glucose stimulation. $n = 4$ wild-type mice; $n = 5$ $\beta7^{-/-}$ mice. **i**, Insulin-tolerance test in wild-type and $\beta7^{-/-}$ mice fed a chow diet. $n = 5$ wild-type mice; $n = 4$ $\beta7^{-/-}$ mice. **j**, Plasma triglyceride (TG) levels of fasted wild-type and $\beta7^{-/-}$ mice. $n = 31$ wild-type mice; $n = 27$ $\beta7^{-/-}$ mice. **k**, Fat-tolerance test in wild-type and $\beta7^{-/-}$ mice fed a chow diet after intraperitoneal injection of 20% intralipid. $n = 5$ mice per group; $^{***}P < 0.001$, two-way analysis of variance (ANOVA). **l**, Hepatic triglyceride secretion. Overnight-fasted wild-type and $\beta7^{-/-}$ mice were injected intraperitoneally with the lipase inhibitor poloxamer 407 (P407) and plasma triglyceride levels were determined at the indicated time points. $n = 4$ wild-type mice; $n = 3$ $\beta7^{-/-}$ mice. Data are mean ± s.e.m., representing biological replicates. $^{*}P < 0.05$, $^{**}P < 0.01$, $^{***}P < 0.001$, $^{****}P < 0.0001$, two-tailed Mann–Whitney *U*-tests unless otherwise indicated.

we noted that $\beta7^{-/-}Ldlr^{-/-}$ mice had lower levels of plasma cholesterol, smaller aortic root lesions and fewer aortic leukocytes after HCD (Extended Data Fig. 4a–d). Finally, we injected anti-integrin β7 antibodies into $Ldlr^{-/-}$ mice and found that these mice had improved glucose tolerance and attenuated atherosclerosis (Extended Data Fig. 4e–g). These data show that integrin β7 deficiency protects against atherosclerosis.

Next, we investigated which cells account for our findings. Intraepithelial lymphocytes that reside in the small intestine had the highest integrin β7 expression (Fig. 4a), in agreement with studies that have shown that integrin β7 guides leukocytes to the gut[16,17]. Although the intestinal intraepithelium had fewer CD3$^+$ cells in $\beta7^{-/-}$ mice (Extended Data Fig. 5a), we nevertheless analysed the relative ability of β7$^+$ cells to enter tissues (Extended Data Fig. 5b). The blood contained $\beta7^{-/-}$ and wild-type cells in similar proportions (Fig. 4b) and—although many tissues accumulated $\beta7^{-/-}$ and wild-type cells in similar, albeit varied, proportions—considerably fewer $\beta7^{-/-}$ cells accumulated in the gut and particularly in the small intestine intraepithelium (Fig. 4b and Extended Data Fig. 5b). These findings therefore confirm that integrin β7 directs leukocytes to the gut.

We show that the leukocytes that rely on integrin β7 influx to the gut are αβ and γδ T cells (Fig. 4c), B cells and myeloid cells (Extended Data Fig. 5c). Notably, $\beta7^{-/-}$ mice had similar numbers of leukocytes as wild-type mice in metabolically important organs such as the liver and pancreas (Extended Data Fig. 5d, e). Although T cells were the most numerous integrin β7-dependent population that was assessed in the gut, we nevertheless tested which of the three populations (αβ and γδ T cells, B cells or myeloid cells) mediated the metabolic effects. We therefore generated five different mixed chimeric groups of mice ($\beta7^{-/-}$ wild-type, $\beta7^{-/-}Tcrb^{-/-}$ (hereafter $\beta7^{-/-}\beta TCR^{-/-}$), $\beta7^{-/-}Tcrd^{-/-}$ (hereafter $\beta7^{-/-}\gamma\delta TCR^{-/-}$), $\beta7^{-/-}Ighm^{tm1Cgn}$ (hereafter $\beta7^{-/-}\mu$MT) and $\beta7^{-/-}Ccr2^{-/-}$) on a wild-type background and performed a glucose-tolerance test to screen for the metabolic phenotype. We found that specific absence of integrin β7 on either αβ ($\beta7^{-/-}\beta TCR^{-/-}$) or γδ ($\beta7^{-/-}\gamma\delta TCR^{-/-}$) T cells improved glucose tolerance (Fig. 4d), whereas no changes were found in the other mixed chimaeras (Extended Data Fig. 5f). Both $Itgae^{-/-}$ and $Ccr9^{-/-}$ mice[18,19] showed a similar improvement in glucose tolerance (Fig. 4e). Moreover, given the importance of B cells for gut homeostasis[20,21], we analysed the contribution of this lymphocyte population in more detail, but found no differences in glucose tolerance, cholesterolaemia or atherosclerosis (Extended Data Fig. 6), indicating that β7-dependent B cells do not contribute to the metabolic phenotype. These data show that intraepithelial αβ and γδ T cells regulate systemic metabolism.

In response to dietary nutrients, enteroendocrine L-cells in the gut produce the incretin hormone GLP-1, which induces postprandial pancreatic insulin secretion and exerts glucose control[22,23]. GLP-1 mediates various other beneficial effects on metabolism, while its analogue improves cardiovascular outcomes in patients with diabetes[24,25]. We found that bm$\beta7^{-/-}Ldlr^{-/-}$ mice that were fed a HCD had higher levels of fasting GLP-1 in the plasma (Fig. 4f), along with increased gut *Gcg* mRNA levels (Fig. 4g). In addition, $\beta7^{-/-}$ mice had increased levels of GLP-1 compared to wild-type mice that were fed chow or a HFSSD (Extended Data Fig. 7a, b). To test whether αβ and γδ T cells controlled the bioavailability of GLP-1, we measured the expression of the GLP-1 receptor in gut leukocytes and found that natural αβ and

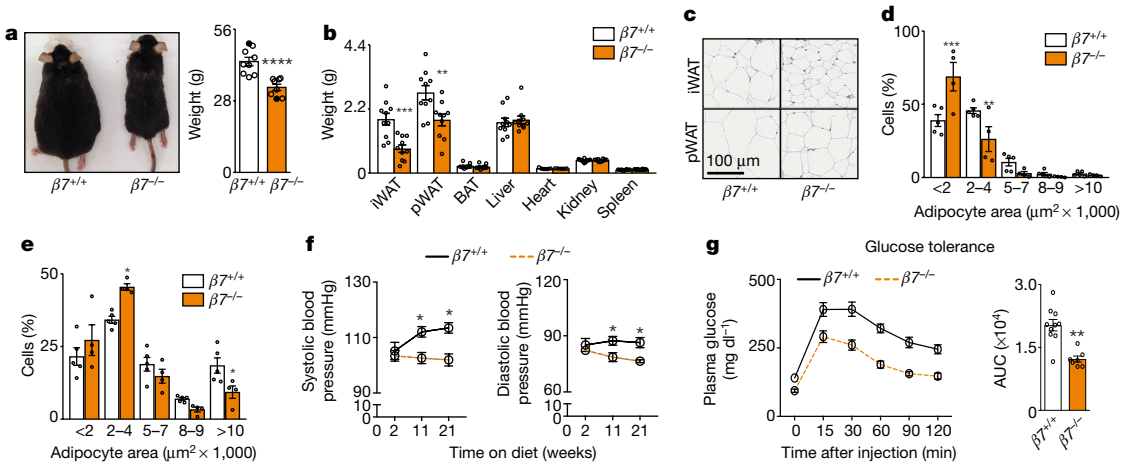

Fig. 2 | Integrin β7 deficiency protects against metabolic syndrome. **a**, Body weights of wild-type and $\beta7^{-/-}$ mice that were fed a HFSSD for 5 months. $n = 9$ wild-type mice; $n = 8$ $\beta7^{-/-}$ mice. Representative images of wild-type and $\beta7^{-/-}$ mice are shown on the left. Black dots denote animals shown in the images. **b**, Tissue weights of wild-type and $\beta7^{-/-}$ mice after 5 months of a HFSSD. $n = 10$ mice per group, except for heart, $n = 5$. **c**, Representative haematoxylin and eosin images of iWAT and pWAT of wild-type ($n = 5$) and $\beta7^{-/-}$ ($n = 4$) mice fed a HFSSD for 5 months. **d**, **e**, Quantification of adipocytes at indicated size ranges in iWAT and pWAT of wild-type and $\beta7^{-/-}$ mice fed a HFSSD for 5 months. $n = 5$ wild-type mice; $n = 4$ $\beta7^{-/-}$ mice. A nonparametric multiple-comparisons test was used. **f**, Blood pressure measurements of mice fed a HFSSD. $n = 5$ mice per group. **g**, Left, glucose-tolerance test using oral glucose gavage (2 g per kg body weight) in wild-type and $\beta7^{-/-}$ mice fed a HFSSD for 5 months. Right, AUC of the glucose-tolerance test. $n = 10$ wild-type mice; $n = 7$ $\beta7^{-/-}$ mice. Data are mean ± s.e.m., representing biological replicates. $^*P < 0.05$, $^{**}P < 0.01$, $^{***}P < 0.001$, $^{****}P < 0.0001$, two-tailed Mann–Whitney *U*-tests unless otherwise indicated.

γδ T cells in wild-type mice showed abundant expression of the GLP-1 receptor, consistent with data from Immgen (http://www.immgen.org/) and a previous study[26] (Fig. 4h). By contrast, the guts of $\beta7^{-/-}$ mice were relatively deficient in expression of the GLP-1 receptor, containing fewer and mostly Glp1r^{low} T cells (Extended Data Figs. 5a, 7c, d). These results indicate that loss of Glp1r^{high} natural IELs is associated with increased plasma levels of the ligand (GLP-1), an observation that is consistent with previous studies that show increased levels of GLP-1 in $Glp1r^{-/-}$ mice[27].

To determine whether loss of the GLP-1 receptor on IELs protects against atherosclerosis through increased systemic levels of GLP-1, we generated mixed chimaeras (bm$Glp1r^{-/-}\beta7^{-/-}$; Fig. 4i) on a $Ldlr^{-/-}$ background. After performing quality-control experiments (Extended Data Figs. 7e, 8a–e), we found that bm$Glp1r^{-/-}\beta7^{-/-}Ldlr^{-/-}$ mice had increased concentrations of GLP-1 (Fig. 4j), were more glucose tolerant (Fig. 4k), less hypercholesterolaemic (Fig. 4l) and developed smaller atherosclerotic lesions (Fig. 4m) with fewer aortic leukocytes (Fig. 4n). Of note, no differences in glucose tolerance and GLP-1 levels were

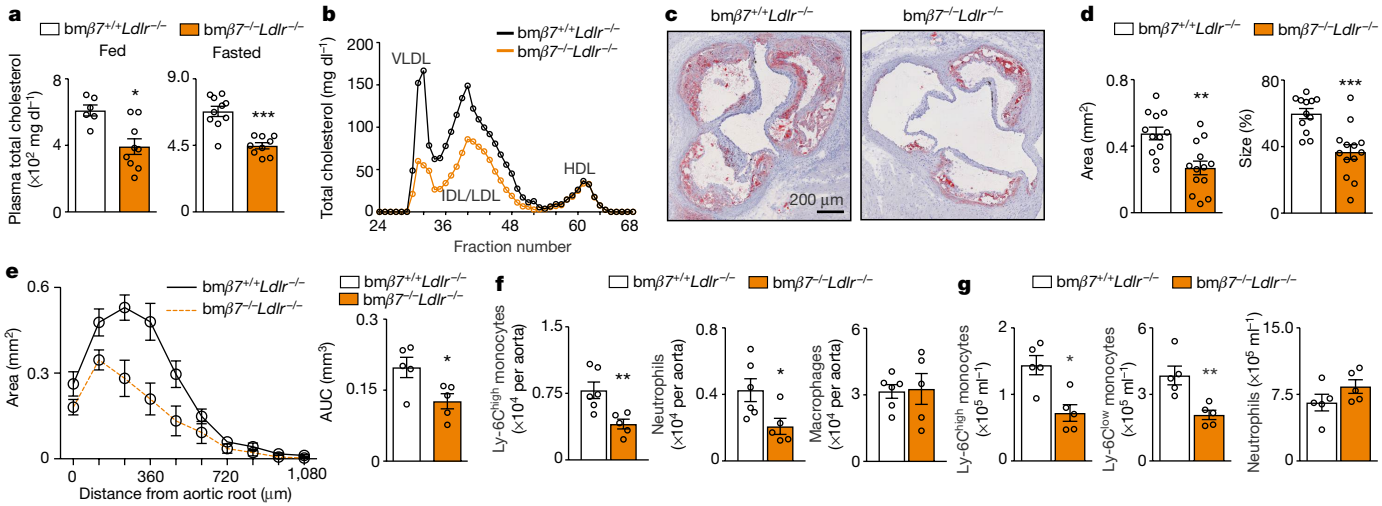

Fig. 3 | Integrin β7 deficiency protects against atherosclerosis. $Ldlr^{-/-}$ mice were lethally irradiated and reconstituted with bone marrow cells from either wild-type (bm$\beta7^{+/+}Ldlr^{-/-}$) or $\beta7^{-/-}$ (bm$\beta7^{-/-}Ldlr^{-/-}$) mice. **a**, Plasma cholesterol in fed and overnight-fasted animals fed a HCD for 14 weeks. $n = 6$ bm$\beta7^{+/+}Ldlr^{-/-}$ mice; $n = 9$ bm$\beta7^{-/-}Ldlr^{-/-}$ fed mice; $n = 10$ bm$\beta7^{+/+}Ldlr^{-/-}$ mice; $n = 9$ bm$\beta7^{-/-}Ldlr^{-/-}$ fasted mice. **b**, Plasma lipoprotein distribution measured by fast-performed liquid chromatography in bm$\beta7^{+/+}Ldlr^{-/-}$ and bm$\beta7^{-/-}Ldlr^{-/-}$ mice. HDL, high-density lipoprotein; IDL, intermediate-density lipoprotein; LDL, low-density lipoprotein; VLDL, very-low-density lipoprotein. Plasma from $n = 5$ mice per group was pooled. **c**, **d**, Representative images (**c**) and quantification (**d**) of oil-red O staining of aortic root sections from bm$\beta7^{+/+}Ldlr^{-/-}$ and bm$\beta7^{-/-}Ldlr^{-/-}$ mice fed a HCD for 14 weeks. $n = 12$ bm$\beta7^{+/+}Ldlr^{-/-}$ mice; $n = 13$ bm$\beta7^{-/-}Ldlr^{-/-}$ mice. **e**, Plaque volumes were calculated by measuring the plaque size at increasing distances from the aortic root. $n = 5$ mice per group; $^*P < 0.05$, two-tailed unpaired Student's *t*-test. **f**, **g**, Leukocyte quantification in aortas (**f**) and blood (**g**) of bm$\beta7^{+/+}Ldlr^{-/-}$ and bm$\beta7^{-/-}Ldlr^{-/-}$ mice fed a HCD for 14 weeks. $n = 6$ bm$\beta7^{+/+}Ldlr^{-/-}$ and $n = 5$ bm$\beta7^{-/-}Ldlr^{-/-}$ in **f**; $n = 5$ mice per group in **g**. Data are mean ± s.e.m., representing biological replicates. $^*P < 0.05$, $^{**}P < 0.01$, $^{***}P < 0.001$, two-tailed Mann–Whitney *U*-tests unless otherwise indicated.

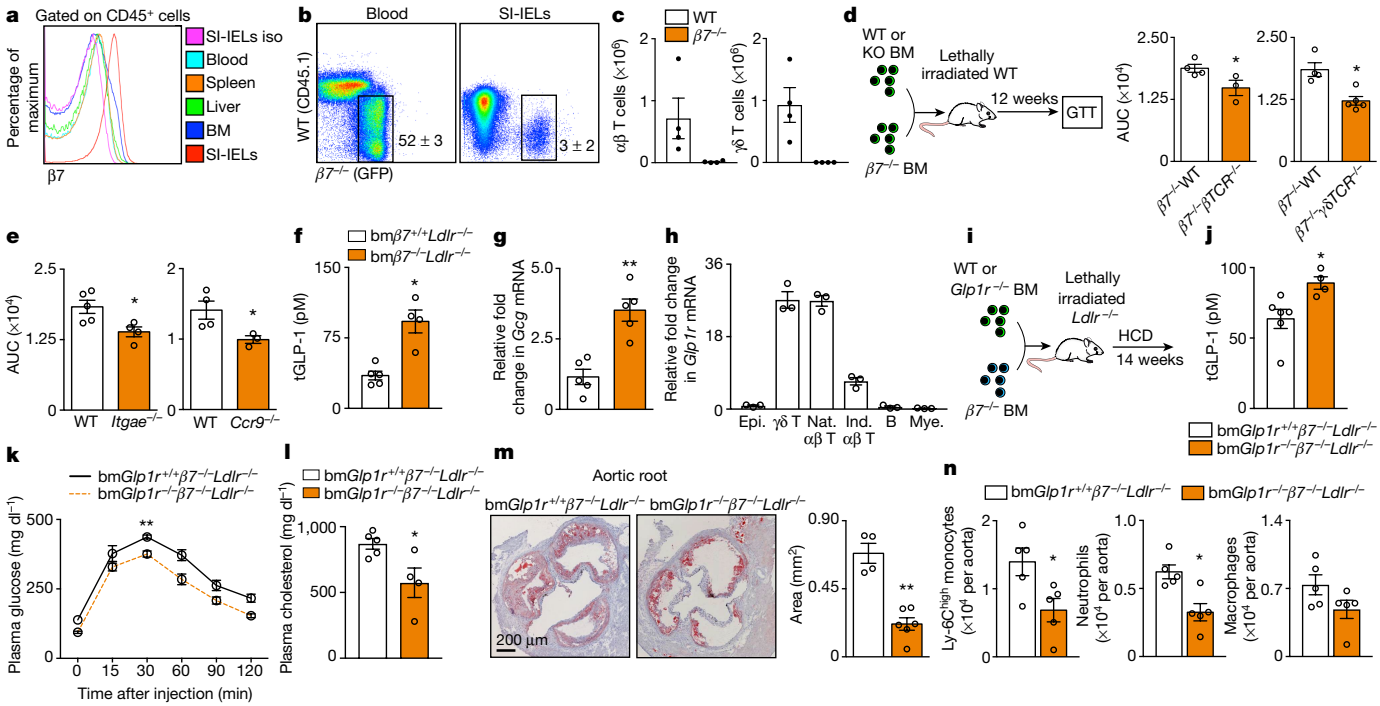

Fig. 4 | Natural IELs calibrate metabolism and protect against cardiovascular disease through GLP-1. a, Histogram (of $n = 4$) showing integrin β7 expression on leukocytes in wild-type mice. BM, bone marrow; iso, isotype control; SI-IELs, small-intestine intraepithelial leukocytes. **b**, Flow cytometry plots showing leukocyte chimerism in blood and among SI-IELs. CD45.2$^+$ mice were lethally irradiated and transplanted with a 1:1 ratio mixture of GFP$^+$*β7*$^{-/-}$ and CD45.1$^+$ wild-type bone marrow cells. **c**, T cell quantification in small intestine in the same mice as **b**. $n = 4$ recipient mice. **d**, Wild-type mice were lethally irradiated and reconstituted with bone marrow cell mixtures to generate mixed chimeric mice. Data show glucose-tolerance tests (GTT) and the AUC in *β7*$^{-/-}$ wild-type (WT) ($n = 4$ mice), *β7*$^{-/-}$*βTCR*$^{-/-}$ ($n = 3$ mice), and *β7*$^{-/-}$*γδTCR*$^{-/-}$ ($n = 5$ mice) mice. KO indicates knockout (either *βTCR*$^{-/-}$ or *γδTCR*$^{-/-}$) bone marrow. **e**, Glucose-tolerance test (intraperitoneal injection) in wild-type ($n = 4$ and 5 mice) and *Itgae*$^{-/-}$ ($n = 4$ mice) or *Ccr9*$^{-/-}$ mice ($n = 3$ mice). **f**, **g**, Fasting plasma total GLP-1 (tGLP-1) levels (**f**) and *Gcg* mRNA expression (**g**) in the ileum of bm*β7*$^{+/+}$*Ldlr*$^{-/-}$ ($n = 5$ mice) and bm*β7*$^{-/-}$*Ldlr*$^{-/-}$ ($n = 4$ and 5 mice) mice fed a HCD for 14 weeks. **h**, *Glp1r* in sorted IELs from wild-type mice. $n = 3$ mice. Epi., epithelial cells; Mye., myeloid cells; Nat., natural; Ind., induced. **i**, Experimental set-up for generating mixed bone marrow chimaeras. **j**, Fasting plasma total GLP-1 levels. $n = 6$ bm*Glp1r*$^{+/+}$*β7*$^{-/-}$*Ldlr*$^{-/-}$ mice; $n = 4$ bm*Glp1r*$^{-/-}$*β7*$^{-/-}$*Ldlr*$^{-/-}$ mice. **k**, Glucose-tolerance test. $n = 5$ mice. **l**, Plasma cholesterol. $n = 5$ bm*Glp1r*$^{+/+}$*β7*$^{-/-}$*Ldlr*$^{-/-}$ mice; $n = 4$ bm*Glp1r*$^{-/-}$*β7*$^{-/-}$*Ldlr*$^{-/-}$ mice. $^*P < 0.05$, two-tailed unpaired Student's *t*-test. **m**, Representative images and quantification of oil-red O-stained aortic roots. $n = 4$ bm*Glp1r*$^{+/+}$*β7*$^{-/-}$*Ldlr*$^{-/-}$ mice; $n = 6$ bm*Glp1r*$^{-/-}$*β7*$^{-/-}$*Ldlr*$^{-/-}$ mice. **n**, Quantification of the number of leukocytes in aortas. $n = 5$ mice. **k**–**n**, Mice were fed a HCD. Data are mean ± s.e.m., representing biological replicates. $^*P < 0.05$, $^{**}P < 0.01$, two-tailed Mann–Whitney *U*-tests unless otherwise indicated.

apparent between *Glp1r*$^{-/-}$ and wild-type chimaeras on a wild-type (that is, not *Ldlr*$^{-/-}$) background, although we did see differences in the *Glp1r*$^{-/-}$*β7*$^{-/-}$ mixed chimaeras (Extended Data Fig. 8f–i). By contrast, we found attenuated atherosclerosis in *Ldlr*$^{-/-}$ mice that received the GLP-1 receptor agonist exendin-4 (Extended Data Fig. 8j, k), consistent with previous data generated in *Apoe*$^{-/-}$ mice[28,29].

Finally, we reasoned that Glp1r^{high} IELs may be limiting the bioavailability of GLP-1 by several non-mutually exclusive mechanisms. First, we found that *β7*$^{-/-}$ mice had an increased number of GLP-1-producing L-cells, suggesting that Glp1r^{high} IELs may be controlling GLP-1 production (Extended Data Fig. 9a). Second, we confirmed that the GLP-1 receptor in Glp1r^{high} IELs is functional, can bind to, capture (Extended Data Fig. 9b) and control the bioavailability of GLP-1 (Extended Data Fig. 9c–f). These results indicate that the loss of the GLP-1 receptor in IELs triggers a systemic response and limits development of cardiovascular disease through regulation of GLP-1 availability (Extended Data Fig. 10).

In the gut, T cells help to maintain barrier integrity via various pleiotropic functions. Here we identified β7$^+$ IELs as critical gatekeepers of dietary metabolism. Although the evolution of regulatory mechanisms that sense nutrient availability and regulate energy disposal and storage should offer a survival advantage over organisms that indiscriminately metabolize and expend their ingested energy, such mechanisms may have adverse effects if they become too dominant. Future studies will therefore need to investigate the function of IELs in numerous contexts to determine whether specific targeting of this population or its products can mitigate cardiometabolic diseases.

Online content

Any methods, additional references, Nature Research reporting summaries, source data, statements of data availability and associated accession codes are available at https://doi.org/10.1038/s41586-018-0849-9.

Received: 1 December 2017; Accepted: 5 December 2018;
Published online: 30 January 2019

1. Begg, D. P. & Woods, S. C. The endocrinology of food intake. *Nat. Rev. Endocrinol.* **9**, 584–597 (2013).
2. Drucker, D. J. The cardiovascular biology of glucagon-like peptide-1. *Cell Metab.* **24**, 15–30 (2016).
3. Cerf-Bensussan, N., Bègue, B., Gagnon, J. & Meo, T. The human intraepithelial lymphocyte marker HML-1 is an integrin consisting of a β7 subunit associated with a distinctive α chain. *Eur. J. Immunol.* **22**, 273–277 (1992).
4. Cheroutre, H., Lambolez, F. & Mucida, D. The light and dark sides of intestinal intraepithelial lymphocytes. *Nat. Rev. Immunol.* **11**, 445–456 (2011).
5. Holzmann, B., McIntyre, B. W. & Weissman, I. L. Identification of a murine Peyer's patch—specific lymphocyte homing receptor as an integrin molecule with an α chain homologous to human VLA-4α. *Cell* **56**, 37–46 (1989).
6. Holzmann, B. & Weissman, I. L. Peyer's patch-specific lymphocyte homing receptors consist of a VLA-4-like α chain associated with either of two integrin β chains, one of which is novel. *EMBO J.* **8**, 1735–1741 (1989).
7. Parker, C. M. et al. A family of β$_7$ integrins on human mucosal lymphocytes. *Proc. Natl Acad. Sci. USA* **89**, 1924–1928 (1992).
8. Gorfu, G., Rivera-Nieves, J. & Ley, K. Role of β7 integrins in intestinal lymphocyte homing and retention. *Curr. Mol. Med.* **9**, 836–850 (2009).

9. Buck, M. D., Sowell, R. T., Kaech, S. M. & Pearce, E. L. Metabolic instruction of immunity. *Cell* **169**, 570–586 (2017).
10. Johnson, A. M. & Olefsky, J. M. The origins and drivers of insulin resistance. *Cell* **152**, 673–684 (2013).
11. Lumeng, C. N. & Saltiel, A. R. Inflammatory links between obesity and metabolic disease. *J. Clin. Invest.* **121**, 2111–2117 (2011).
12. Odegaard, J. I. & Chawla, A. The immune system as a sensor of the metabolic state. *Immunity* **38**, 644–654 (2013).
13. Swirski, F. K. & Nahrendorf, M. Leukocyte behavior in atherosclerosis, myocardial infarction, and heart failure. *Science* **339**, 161–166 (2013).
14. Swirski, F. K. et al. Ly-6C^{hi} monocytes dominate hypercholesterolemia-associated monocytosis and give rise to macrophages in atheromata. *J. Clin. Invest.* **117**, 195–205 (2007).
15. Hilgendorf, I. & Swirski, F. K. Making a difference: monocyte heterogeneity in cardiovascular disease. *Curr. Atheroscler. Rep.* **14**, 450–459 (2012).
16. Berlin, C. et al. $\alpha4\beta7$ integrin mediates lymphocyte binding to the mucosal vascular addressin MAdCAM-1. *Cell* **74**, 185–195 (1993).
17. Wagner, N. et al. Critical role for $\beta7$ integrins in formation of the gut-associated lymphoid tissue. *Nature* **382**, 366–370 (1996).
18. Schön, M. P. et al. Mucosal T lymphocyte numbers are selectively reduced in integrin α_E (CD103)-deficient mice. *J. Immunol.* **162**, 6641–6649 (1999).
19. Uehara, S., Grinberg, A., Farber, J. M. & Love, P. E. A role for CCR9 in T lymphocyte development and migration. *J. Immunol.* **168**, 2811–2819 (2002).
20. Lycke, N. Y. & Bemark, M. The regulation of gut mucosal IgA B-cell responses: recent developments. *Mucosal Immunol.* **10**, 1361–1374 (2017).
21. Fagarasan, S. & Honjo, T. Intestinal IgA synthesis: regulation of front-line body defences. *Nat. Rev. Immunol.* **3**, 63–72 (2003).
22. Baggio, L. L. & Drucker, D. J. Biology of incretins: GLP-1 and GIP. *Gastroenterology* **132**, 2131–2157 (2007).
23. Kahles, F. et al. GLP-1 secretion is increased by inflammatory stimuli in an IL-6-dependent manner, leading to hyperinsulinemia and blood glucose lowering. *Diabetes* **63**, 3221–3229 (2014).
24. Marso, S. P. et al. Liraglutide and cardiovascular outcomes in type 2 diabetes. *N. Engl. J. Med.* **375**, 311–322 (2016).
25. Marso, S. P. et al. Semaglutide and cardiovascular outcomes in patients with type 2 diabetes. *N. Engl. J. Med.* **375**, 1834–1844 (2016).
26. Yusta, B. et al. GLP-1R agonists modulate enteric immune responses through the intestinal intraepithelial lymphocyte GLP-1R. *Diabetes* **64**, 2537–2549 (2015).
27. Lamont, B. J. et al. Pancreatic GLP-1 receptor activation is sufficient for incretin control of glucose metabolism in mice. *J. Clin. Invest.* **122**, 388–402 (2012).
28. Arakawa, M. et al. Inhibition of monocyte adhesion to endothelial cells and attenuation of atherosclerotic lesion by a glucagon-like peptide-1 receptor agonist, exendin-4. *Diabetes* **59**, 1030–1037 (2010).
29. Nagashima, M. et al. Native incretins prevent the development of atherosclerotic lesions in apolipoprotein E knockout mice. *Diabetologia* **54**, 2649–2659 (2011).

Acknowledgements This work was supported by NIH grants R35 HL135752, R01 HL128264, P01 HL131478, the AHA EIA and the Patricia and Scott Eston MGH Research Scholar (to F.K.S.). S.H. was supported by an AHA Postdoctoral Award (16POST27250124); F.K. and W.C.P. by the German Research Foundation (DFG); S.R. was supported by a postdoctoral fellowship from the Swedish Research Council; M. Nairz was supported by a FWF Erwin Schroedinger Fellowship (J3486-B13); J.E.M. was supported by a NIH training grant (T32 AI118692); L.H. was supported by a Boehringer Ingelheim Fonds MD Fellowship; and D.J.D. was supported by a CIHR grant 154321, the Canada Research Chairs program and a BBDC-Novo Nordisk Chair in Incretin biology. We thank K. Joyes for copy-editing the manuscript.

Reviewer information *Nature* thanks D. Mucida, F. Reimann and the other anonymous reviewer(s) for their contribution to the peer review of this work.

Author contributions S.H. conceived the project, designed and performed experiments, analysed and interpreted data and made the figures; F.K. performed experiments, analysed and interpreted data and made the figures; S.R., M. Nairz, A.A., C.S.M., D.S., A.M.F., C.T.C., J.E.M., C.V., W.C.P., Y.I., G.R.W. and C.F.-H. performed experiments; R.W., P.L., C.F.-H., D.J.D. and M. Nahrendorf provided intellectual input; R.W., C.F.-H., D.J.D. and M. Nahrendorf provided materials; F.K.S. conceived the project, designed experiments, interpreted data and wrote the manuscript. All authors edited the manuscript.

Competing interests The General Hospital Corporation has filed a US patent application 62/771,668 with the US Patent and Trademark office entitled 'Targeting intraepithelial leukocytes for treatment of cardiometabolic diseases', which names F.K.S. and S.H. as inventors. D.J.D. has served as an advisor or consultant to Intarcia, Forkhead Biopharmaceuticals Inc., Kallyope Inc., Merck Research Laboratories, Pfizer Inc., Novo Nordisk Inc. and Zafgen Inc. Mount Sinai receives funding from GSK, Merck and Novo Nordisk for GLP-1-related studies in the Drucker laboratory.

Additional information

Extended data is available for this paper at https://doi.org/10.1038/s41586-018-0849-9.
Supplementary information is available for this paper at https://doi.org/10.1038/s41586-018-0849-9.

Correspondence and requests for materials should be addressed to S.H. or F.K.S.

METHODS

Mice. C57BL/6J (wild-type mice), B6.SJL-Ptprc^{a}Pepc^{b}/BoyJ (CD45.1^{+}), *Itgb7*^{tm1Cgn} (*β7*$^{-/-}$), *Ldlr*^{tm1Her} (*Ldlr*$^{-/-}$), *Tcrb*^{tm1Mom} (*βTCR*$^{-/-}$), *Tcrd*^{tm1Mom} (*γδTCR*$^{-/-}$), *Ccr2*^{tm1Ifc} (*Ccr2*$^{-/-}$), *Ighm*^{tm1Cgn} (μMT), *Ccr9*^{tm1Lov} (*Ccr9*$^{-/-}$), *Itgae*^{tm1Cmp} (*Itgae*$^{-/-}$), and C57BL/6-Tg(UBC-GFP)30Scha/J (GFP^{+}) mice were purchased from The Jackson Laboratory. *Glp1r*$^{-/-}$ mice on the C57BL/6 background were bred in-house as described[30]. Unless otherwise indicated, age- and sex-matched animals were used starting at 8–12 weeks of age. Female mice were used for experiments in Fig. 1h, k, l, 4e, and Extended Data Figs. 1g, 4c, d. A mixture of sexes was used in Fig. 1j. Male mice were used in all other experiments. Investigators were blinded to group allocation during data collection and analysis. Where appropriate, animals were randomly assigned to interventions. All protocols were approved by the Animal Review Committee at Massachusetts General Hospital (protocols 2011N000035 and 2015N000044) and were in compliance with relevant ethical regulations.

Animal models and in vivo interventions. *Diet.* For studies on metabolic syndrome, wild-type and *β7*$^{-/-}$ mice were fed a HFSSD (Research Diets D12331). For studies on atherosclerosis, bone marrow chimaeras on the *Ldlr*$^{-/-}$ background or double knockouts were fed a HCD (Research Diets D12108C). HFSSD-fed and HCD-fed mice were single- or group-housed on a 12-h:12-h light:dark cycle at 22 °C with free access to food and water. HFSSD-fed mice were maintained under these conditions for 21 weeks and HCD-fed mice for 14 weeks. For studies on glucose tolerance in thermoneutrality, wild-type mice and *β7*$^{-/-}$ mice were housed for 3 days in a 12-h:12-h light:dark cycle at 30 °C with free access to food and water. For studies on microbiota, mice were treated with an antibiotics cocktail (0.1% ampicillin, 0.1% metronidazole, 0.05% vancomycin and 0.1% neomycin) in drinking water for 4 weeks and an equal number of 8-week-old wild-type and *β7*$^{-/-}$ mice with the same day of birth were co-housed for 4 weeks.

Bone marrow transplantation. Naive C57BL/6 or *Ldlr*$^{-/-}$ mice were lethally irradiated (950 cGy) and reconstituted with indicated bone marrow cells to generate different chimaera groups: (i) bm*β7*$^{+/+}$*Ldlr*$^{-/-}$ and bm*β7*$^{-/-}$*Ldlr*$^{-/-}$ (irradiated *Ldlr*$^{-/-}$ mice reconstituted with either wild-type or *β7*$^{-/-}$ bone marrow); (ii) bm*β7*$^{+/+}$CD45.1^{+} or bm*β7*$^{-/-}$GFP^{+}*Ldlr*$^{-/-}$(irradiated *Ldlr*$^{-/-}$ mice reconstituted with a 1:1 bone marrow mixture of CD45.1^{+} wild-type and GFP^{+}*β7*$^{-/-}$ bone marrow); (iii) bm*β7*$^{+/+}$CD45.1^{+} or bm*β7*$^{-/-}$GFP^{+} (irradiated wild-type mice reconstituted with a 1:1 bone marrow mixture of CD45.1^{+} wild-type and GFP^{+}*β7*$^{-/-}$ bone marrow); (iv) *β7*$^{-/-}$ wild-type, *β7*$^{-/-}$*βTCR*$^{-/-}$, and *β7*$^{-/-}$*γδTCR*$^{-/-}$ (irradiated wild-type mice reconstituted with 1:1 bone marrow mixtures of *β7*$^{-/-}$ and wild-type, *β7*$^{-/-}$ and *βTCR*$^{-/-}$, and *β7*$^{-/-}$ and *γδTCR*$^{-/-}$, respectively); (v) bm*Glp1r*$^{+/+}$*β7*$^{-/-}$*Ldlr*$^{-/-}$ and bm*Glp1r*$^{-/-}$*β7*$^{-/-}$*Ldlr*$^{-/-}$ (irradiated *Ldlr*$^{-/-}$ mice reconstituted with 1:1 bone marrow mixtures of wild-type and *β7*$^{-/-}$, and *Glp1r*$^{-/-}$ and *β7*$^{-/-}$, respectively); (vi) bm*Glp1r*$^{+/+}$ and bm*Glp1r*$^{-/-}$ (irradiated wild-type mice reconstituted with either wild-type or *Glp1r*$^{-/-}$ bone marrow); and (vii) bm*Glp1r*$^{+/+}$GFP^{+} and bm*Glp1r*$^{-/-}$GFP^{+} (irradiated wild-type mice reconstituted with 1:1 bone marrow mixtures of wild-type and GFP^{+}, and *Glp1r*$^{-/-}$ and GFP^{+}, respectively); (viii) bm*β7*$^{-/-}$*Ccr2*$^{-/-}$, bm*β7*$^{-/-}$ μMT, and bm*β7*$^{-/-}$ wild-type (irradiated wild-type mice reconstituted with 1:1 bone marrow mixtures of *β7*$^{-/-}$ and *Ccr2*$^{-/-}$, *β7*$^{-/-}$ and μMT, and *β7*$^{-/-}$ and wild-type, respectively; (ix) bm*β7*$^{-/-}$ wild-type *Ldlr*$^{-/-}$ or bm*β7*$^{-/-}$ μMT *Ldlr*$^{-/-}$ (irradiated *Ldlr*$^{-/-}$ mice reconstituted with 1:1 bone marrow mixtures of *β7*$^{-/-}$ and wild-type, and *β7*$^{-/-}$ and μMT, respectively.

Anti-integrin β7 antibody treatment. Ldlr$^{-/-}$ mice on a HCD were treated with anti-integrin β7 antibodies (FIB504, BioxCell) or IgG isotype control (2A3, BioxCell) by intraperitoneal injection for 14 weeks for quantification of atherosclerotic plaque size after euthanasia (500 μg per mouse per week).

Glp1r agonist treatment. Ldlr$^{-/-}$ mice were treated with the Glp1r agonist exendin-4 (Abcam) at a dose of 100 μg per kg per day via osmotic minipumps (Alzet). After 8 weeks on a HCD, mice were euthanized for atherosclerotic lesion quantification.

Metabolic measurements. *CLAMS.* A comprehensive laboratory animal monitoring system (CLAMS, The Columbus Instruments) was used at the Joslin Diabetes Center Animal Physiology Core to simultaneously measure a series of metabolic parameters including energy expenditure (heat production), oxygen consumption (V_{O_2}), carbon dioxide production (V_{CO_2}), respiratory exchange ratio, food consumption and locomotor activity levels.

Blood pressure measurements. Systolic and diastolic blood pressures were measured using a non-invasive tail-cuff system (Kent Scientific). Mice were initially acclimatized to the instrument for three consecutive days before the measurements.

[^{18}F]FDG PET/CT. The uptake and distribution of glucose in vivo were determined by [^{18}F]FDG and non-invasive, high-resolution PET/CT imaging and ex vivo biodistribution. In brief, mice were anaesthetized with isoflurane and injected intravenously through the tail vein with around 200 μCi of tracer diluted to a final volume of 150 μl in isotonic saline. Following a 60-min absorption period, mice were imaged on a Siemens Inveon small-animal integrated PET/CT scanner. The CT was acquired over 360 projections using a 80 kV, 1 μA X-ray tube operating at 80 kilovoltage peak (kVp) and 500 μA on a CMOS detector and reconstructed using a modified Feldkamp cone beam reconstruction algorithm (COBRA, Exxim Computing Corporation). A 20-min PET image was acquired and reconstructed using the ordered subsets expectation maximization followed by maximum a posteriori. Regions of interest were manually drawn for standard uptake value calculations. After imaging, animals were euthanized and tissues were collected for biodistribution analysis using gamma well counting on a 20% window on the 511 keV photopeak (Wizard2, PerkinElmer). [^{18}F]FDG levels were normalized to the weight of resected tissue and expressed as the percentage injected dose per gram tissue weight.

Glucose- and insulin-tolerance tests. For glucose- and insulin-tolerance tests, overnight-fasted mice were injected intraperitoneally or by oral gavage with glucose (2 g per kg body weight) or injected intraperitoneally with insulin (0.75 U per kg body weight). Blood glucose levels were measured at the basal level and at 15, 30, 60, 90 and 120 min after glucose or insulin administration using One Touch Ultra2 Blood Glucose Meter (OneTouch, LifeScan).

Fat-tolerance test. Overnight-fasted mice were injected intraperitoneally with 200 μl 20% Intralipid (vol/vol) fat emulsion (Sigma, MA), and blood that was drawn from the retroorbital plexus at the indicated time points for triglyceride measurement using the L-Type Triglyceride M kit (Wako Diagnostics, VA). To measure hepatic lipid export, overnight-fasted mice were injected with 1 g per kg poloxamer 407 (Pluronic F-127, Sigma) and plasma was collected at the indicated time points for triglyceride analysis.

Fat absorption test. To measure fat absorption in the gut, overnight-fasted mice were injected intraperitoneally with 1 g per kg poloxamer 407. After 1 min, the mice were gavaged with 0.4 ml corn oil. Plasma was collected at baseline as well as at the indicated time points after gavage for analysis of triglyceride levels.

FPLC. Mice were fasted for 12–16 h overnight before blood samples were collected by retro-orbital venous plexus puncture, after which plasma was separated by centrifugation. The lipid distribution in plasma lipoprotein fractions was assessed by fast-performed liquid chromatography (FPLC) gel filtration with 2 Superose 6 HR 10/30 columns (Pharmacia Biotech). Total plasma cholesterol in each fraction was enzymatically measured (Wako Pure Chemicals).

Cholesterol. Plasma was collected from overnight-fasted or non-fasted mice that were fed a HCD for 14 weeks, and plasma total cholesterol was determined by a Cholesterol E kit (Wako Diagnostics).

Gut permeability test. Overnight-fasted mice were administered through oral gavage with fluorescein isothiocyanate (FITC)–dextran (Sigma-Aldrich) at a dose of 12 mg per mouse, and plasma was collected 4 h later for fluorescence intensity measurement. A mouse model of colitis in which a mouse was treated with dextran sulfate sodium salt (36–50 kDa, MP Biomedicals) in drinking water for 6 days was used as a positive control for gut barrier disruption.

Cells. *Cell collection.* Peripheral blood was collected by retro-orbital bleeding and red blood cells were lysed in RBC lysis buffer (Biolegend). Aortas were excised after PBS perfusion (Thermo Fisher Scientific), minced and digested with 450 U ml^{-1} collagenase I, 125 U ml^{-1} collagenase XI, 60 U ml^{-1} DNase I and 60 U ml^{-1} hyaluronidase (Sigma-Aldrich) in PBS for 40 min at 37 °C. Total viable cell numbers were counted using trypan blue (Cellgro, Mediatech). Small-intestine IELs were isolated as follows: after excision of the small intestine, the Peyer's patches were removed under a microscope and the gut was cut open longitudinally to wash off the lumen contents in HBSS buffer. The gut was then cut into 1–2-cm pieces and subjected to 3× dissociation in EDTA-containing buffer (7.5 mM HEPES, 2% FCS, 2 mM EDTA, 10,000 U ml^{-1} penicillin–streptomycin, 50 μg ml^{-1} gentamycin in HBSS; all Thermo Fisher Scientific) in a shaker at 37 °C for 15 min. After dissociation the IELs were collected by filtering the lamina propria through a mesh.

Cell sorting. The IEL flow through after dissociation was further subjected to Percoll (GE Healthcare Bio-Sciences) grade centrifugation to remove the mucus. Single-cell suspensions of IELs from indicated animals were then stained to identify indicated cell populations. Cells were sorted on a FACS Aria II cell sorter (BD Biosciences) directly into either RLT buffer for subsequent RNA isolation or into collection medium for ex vivo manipulations.

Flow cytometry. Single-cell suspensions were stained in PBS supplemented with sterile 2% FBS and 0.5% BSA. The following monoclonal antibodies were used for flow cytometric analysis: anti-integrin β7 (clone FIB27), anti-CD45 (30-F11), anti-CD45.1 (clone A20), anti-CD45.2 (clone 104), anti-CD3 (clone 17A2), anti-CD90.2 (clone 53-2.1), anti-CD19 (clone 6D5), anti-B220 (clone RA3-6B2), anti-NK1.1 (clone PK136), anti-Ly-6G (clone 1A8), anti-Ly-6C (AL-21), anti-MHCII (clone AF6-120.1), anti-F4/80 (clone BM8), anti-CD11b (clone M1/70), anti-CD5 (clone 53-7.3), anti-βTCR (clone H57-597), anti-γδTCR (clone GL3), anti-CD326 (clone G8.8), anti-IgA (C10-3), anti-IgD (11-26c.2a), anti-CD115 (clone AFS98), and anti-CX3CR1 (clone SA011F11). Antibodies were all purchased from BioLegend except anti-IgA (BD Biosciences). Viable cells were identified as unstained with Zombie Aqua (Biolegend). Cells were defined as: (i) Ly-6C^{high} monocytes (CD45^{+}Lin^{-}CD11b^{+}F4/80^{-}Ly-6C^{high}); (ii) neutrophils

($CD45^+CD11b^+Lin^+F4/80^-$); (iii) macrophages ($CD45^+Lin^-CD11b^+F4/80^+Ly\text{-}6C^{low}$); (iv) epithelial cells ($CD45^-CD326^+CD3^-$); or (v) myeloid cells ($CD45^+CD3^-CD11b^+$). Lineages were defined as: Lin: CD3, CD90.2, CD19, B220, NK1.1, Ter119, Ly-6G. Data were acquired on a LSRII (BD Biosciences) and analysed with FlowJo (Tree Star).

Cell culture. For all experiments, cells or ex vivo ileum tissues were kept in a humidified 5% CO_2 incubator at 37 °C. (i) For in vitro GLP-1 receptor agonist-binding experiments, small-intestinal IELs were isolated and incubated with 50 pM fluorescently labelled GLP-R agonist exendin-4 Cys40SeTau647 for 1 h, and IEL subsets were gated as follows: natural, $Glp1r^{high}$ IELs ($CD45^+CD3^+CD90.2^-CD5^-$); induced, $Glp1r^{low}$ IELs ($CD45^+CD3^+CD90.2^+CD5^+$), non-T cells ($CD45^+CD3^-$), and epithelial cells ($CD45^-CD326^+CD3^-$). The binding capacity was analysed for exendin-4 Cys40SeTau647 by flow cytometry. (ii) For in vitro co-culture experiments, GLP-1-producing L-cells (GLUTag cells that were provided by D.J.D., authenticated multiple times and tested for mycoplasma) were cultured together with sorted $Glp1r^{high}$ or $Glp1r^{low}$ IELs in DMEM and GlutaMAX-I with glucose 1 g l^{-1} (Invitrogen) supplemented with 10% FBS and 1% penicillin–streptomycin (10^3 GLUTag cells and 10^5 IELs in a 96-well plate in 200 μl medium per well). After 24 h, the concentration of GLP-1 in the supernatant was measured using a total GLP-1 enzyme-linked immunosorbent assay (ELISA) kit (Millipore). In some experiments, the GLP-1 receptor agonist exendin-4 (Abcam) was added to co-culture wells (100 nM). (iii) In the case of two-step ex vivo experiments, sorted $Glp1r^{high}$ IELs were incubated with exendin-4 (100 nM) or control. After 24 h, samples were centrifuged (300*g*, 5 min) and supernatants were transferred to ileum ex vivo sections of previously euthanized wild-type mice. GLP-1 levels were determined 24 h later from ex vivo supernatants. (iv) In an ex vivo GLP-1 receptor-inhibition experiment, whole ileum preparations of wild-type or $\beta7^{-/-}$ mice were treated with the GLP-1 receptor antagonist exendin-9 (100 nM) or control. After 24 h the concentration of GLP-1 in the supernatant was measured using a total GLP-1 ELISA kit (Millipore).

Molecular biology. *PCR.* Total RNA was isolated using the RNeasy Mini Kit (Qiagen) according to the manufacturer's instructions. cDNA was generated from 1 μg of total RNA per sample using the High Capacity cDNA Reverse Transcription Kit (Applied Biosystems). Quantitative real-time TaqMan PCR was performed using the following TaqMan primers (Applied Biosystems): *Glp1r* (Mm00445292_m1), *Gcg* (Mm00801714_m1) and housekeeping gene actin (*Actb*) (Mm02619580_g1). PCR was run on a 7500 thermal cycler (Applied Biosystems) and data were quantified with the $2^{-\Delta C_t}$ method.

ELISA. Total GLP-1 levels were measured in plasma of overnight-fasted mice or during oral glucose-tolerance tests using a commercial ELISA kit (Millipore) according to the manufacturer's instructions. Gut IgA was retrieved by flushing the lumens of dissected guts with 5 ml PBS, and both gut flush IgA and plasma IgA was detected using mouse IgA ELISA kit (Bethyl Laboratories).

Histology. *Adipose tissue.* iWAT and pWAT were excised, fixed in 10% formalin solution and paraffin-embedded. Haematoxylin and eosin staining was performed to assess overall tissue morphology. The adipocyte size distribution was determined with the NIH ImageJ program.

Aortas. Aortic roots were dissected, embedded in Tissue-Tek OCT compound (Sakura Finetek) and frozen in 2-methylbutane (Fisher Scientific) cooled with dry ice. For comparisons of lesion sizes between the groups, sections with the maximum lesion area were used. To measure lesion volume, sections were collected at the first appearance of the aortic valves until lesions were no longer visible. Oil-red O staining (Sigma-Aldrich) was performed to visualize lipid content and the lesion size was measured. To quantify lesion macrophage and smooth muscle cell content, immunohistochemistry was performed with anti-CD68 (BioLegend) and anti-Myh11 (Millipore) antibodies. The positive cells were visualized using the Vectastain ABC kit (Vector Laboratories) and AEC substrate (DAKO/Agilent Technologies) and the slides were counterstained with Harris haematoxylin (Sigma-Aldrich). To quantify collagen content, Masson trichrome staining (Sigma-Aldrich) was performed.

Ileum CD3 cell numbers. Small intestines were dissected and cut open. After rinsing away the lumen contents in PBS, ileum was rolled from proximal to distal parts and embedded for histological sectioning. Immunohistochemistry was performed using an anti-CD3 antibody (BioLegend) and $CD3^+$ cells were quantified.

Ileum L-cell numbers. Ileum sections of wild-type and $\beta7^{-/-}$ mice were paraffin-embedded and GLP-1 staining (Abcam) was performed to quantify GLP-1-producing L-cells in the entire ileum of each mouse. A biotinylated secondary antibody and streptavidin DyLight 594 (Vector Laboratories) were applied and nuclei were identified using DAPI (Thermo Fisher Scientific). All histological slides were scanned using a digital slide scanner NanoZoomer 2.0RS (Hamamatsu).

Statistics. Results are shown as mean ± s.e.m. Unless indicated, statistical tests included unpaired, two-tailed Student's *t*-tests and nonparametric Mann–Whitney *U*-tests (when a Gaussian distribution was not assumed). For multiple-comparisons tests, nonparametric tests that compare the mean rank of each group (when a Gaussian distribution was not assumed) were performed. *P* values of 0.05 or less were considered to denote significance.

Reporting summary. Further information on research design is available in the Nature Research Reporting Summary linked to this paper.

Data availability

All relevant data are included in the paper. Source Data are available for Figs. 1–4 and Extended Data Figs. 1–9 in the online version of the paper.

30. Kim, M. et al. GLP-1 receptor activation and Epac2 link atrial natriuretic peptide secretion to control of blood pressure. *Nat. Med.* **19**, 567–575 (2013).

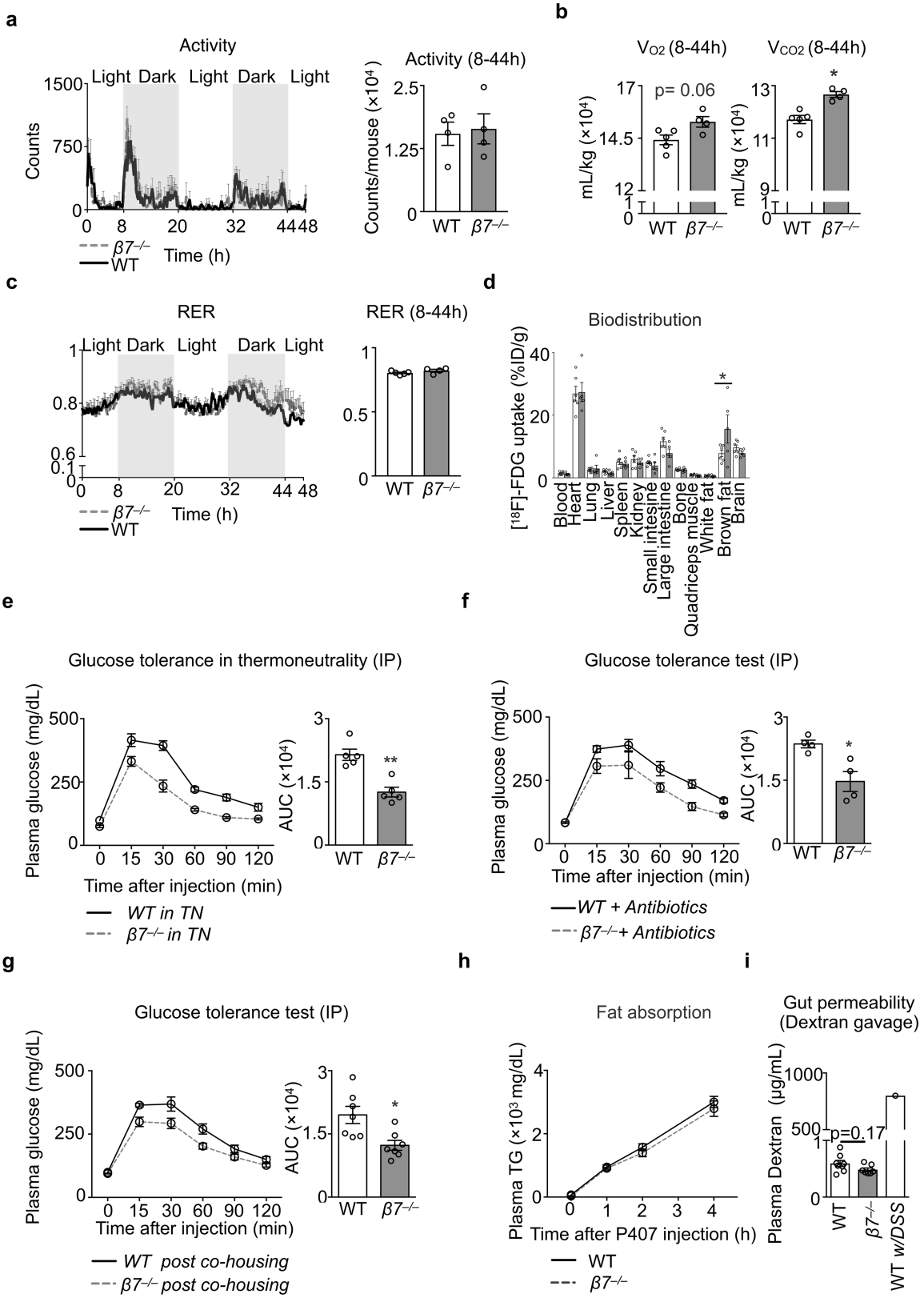

Extended Data Fig. 1 | See next page for caption.

Extended Data Fig. 1 | Effects of integrin β7 deficiency on metabolism. **a**, Metabolic cage measurements of activity in wild-type (WT) and $\beta7^{-/-}$ mice. $n = 4$ mice per group. **b**, O_2 consumption and CO_2 production. $n = 5$ wild-type mice; $n = 4$ $\beta7^{-/-}$ mice. **c**, Respiratory exchange rate (RER) by CLAMS in wild-type and $\beta7^{-/-}$ mice that were fed a chow diet. $n = 5$ wild-type mice; $n = 4$ $\beta7^{-/-}$ mice; $^*P < 0.05$, two-tailed Mann–Whitney *U*-test. **d**, Overnight-fasted wild-type and $\beta7^{-/-}$ mice were administered [^{18}F]FDG. The radioactivity in indicated organs was measured as the percentage injected dose per gram tissue weight (%ID/g). $n = 6$ wild-type mice; $n = 5$ $\beta7^{-/-}$ mice; $^*P < 0.05$, Student's *t*-test. **e**, Wild-type and $\beta7^{-/-}$ mice were housed in thermoneutral (TN) incubators for three days and then subjected to the intraperitoneal (IP) glucose-tolerance test. $n = 5$ mice per group; $^{**}P < 0.01$, two-tailed Mann–Whitney *U*-test. **f**, Wild-type and $\beta7^{-/-}$ mice were treated with antibiotic cocktails in drinking water for 4 weeks and then subjected to the glucose-tolerance test. $n = 4$ mice per group; $^*P < 0.05$, two-tailed Mann–Whitney *U*-test. **g**, Eight-week-old wild-type and $\beta7^{-/-}$ mice were cohoused at a ratio of 1:1 for 4 weeks and then subjected to the glucose-tolerance test. $n = 7$ mice per group; $^*P < 0.05$, two-tailed Mann–Whitney *U*-test. **h**, Fat absorption was analysed using a fat-tolerance test in the presence of P407. $n = 9$ wild-type mice; $n = 6$ $\beta7^{-/-}$ mice. **i**, For assessment of permeability, mice were gavaged with FITC–dextran and fluorescence was measured in the plasma 4 h later. A wild-type mouse subjected to a dextran sulfate sodium (DSS)-induced colitis model was used as a positive control for increased gut permeability. $n = 8$ wild-type mice; $n = 7$ $\beta7^{-/-}$ mice; $P = 0.17$, two-tailed Mann–Whitney *U*-test. Data are mean ± s.e.m.

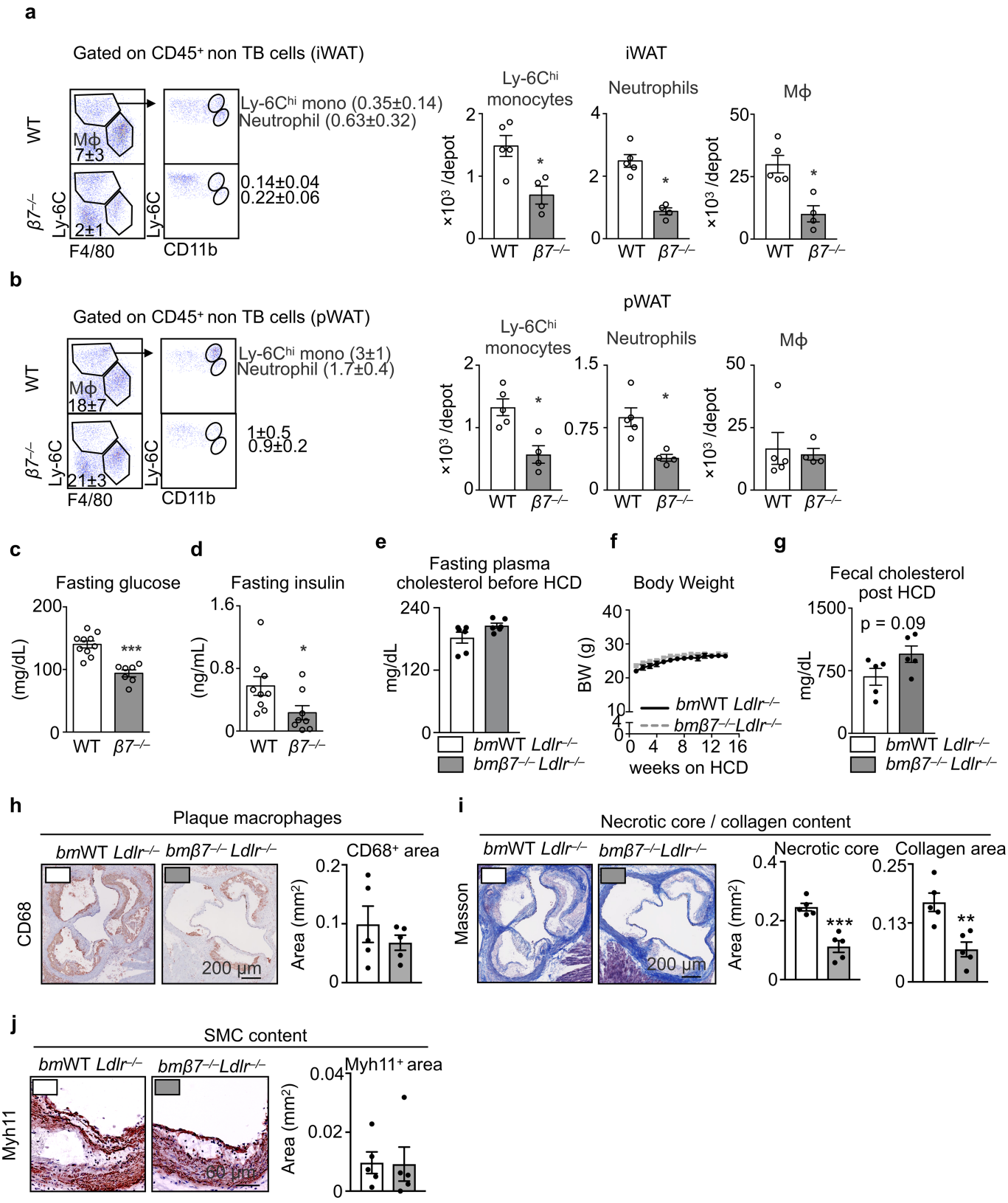

Extended Data Fig. 2 | See next page for caption.

Extended Data Fig. 2 | Effects of integrin β7 deficiency on obesity, cholesterolaemia and atherosclerosis. a, Representative flow cytometry plots gated on $CD45^+$ non-T and B (TB) leukocytes and quantification of Ly-$6C^{high}$ monocytes, neutrophils and macrophages (Mϕ) in iWAT of wild-type and $\beta7^{-/-}$ mice fed a HFSSD for 5 months. $n = 5$ wild-type mice; $n = 4$ $\beta7^{-/-}$ mice; $^*P < 0.05$, two-tailed Mann–Whitney *U*-test. **b**, Representative flow cytometry plots and quantification of Ly-$6C^{high}$ monocytes, neutrophils and macrophages in pWAT of wild-type and $\beta7^{-/-}$ mice fed a HFSSD for 5 months. $n = 5$ wild-type mice; $n = 4$ $\beta7^{-/-}$ mice; $^*P < 0.05$, two-tailed Mann–Whitney *U*-test. **c**, Plasma glucose levels measured in overnight-fasted animals fed a HFSSD for 5 months. $n = 10$ wild-type mice; $n = 7$ $\beta7^{-/-}$ mice; $^{***}P < 0.001$, two-tailed Mann–Whitney *U*-test. **d**, Insulin levels measured in overnight-fasted animals fed a HFSSD for 5 months. $n = 9$ wild-type mice; $n = 8$ $\beta7^{-/-}$ mice; $^*P < 0.05$, two-tailed Mann–Whitney *U*-test. **e**, Fasting plasma total cholesterol levels of mice fed a chow diet. $n = 6$ mice per group. **f**, Body weight changes during a 14-week HCD diet of bm$\beta7^{+/+}Ldlr^{-/-}$ and bm$\beta7^{-/-}Ldlr^{-/-}$ mice. $n = 5$ mice per group. **g**, Faecal cholesterol levels in bm$\beta7^{+/+}Ldlr^{-/-}$ and bm$\beta7^{-/-}Ldlr^{-/-}$ mice after a 14-week HCD diet. $n = 5$ mice per group; $P = 0.09$, two-tailed unpaired Student's *t*-test. **h**–**j**, Representative images and histological quantification of macrophages (**h**), collagen content and necrotic core size (**i**) and smooth muscle cell content (**j**) of bm$\beta7^{+/+}Ldlr^{-/-}$ and bm$\beta7^{-/-}Ldlr^{-/-}$ mice after 14 weeks on a HCD. $n = 5$ mice per group; $^{**}P < 0.01$, $^{***}P < 0.001$, two-tailed unpaired Student's *t*-test. Data are mean ± s.e.m.

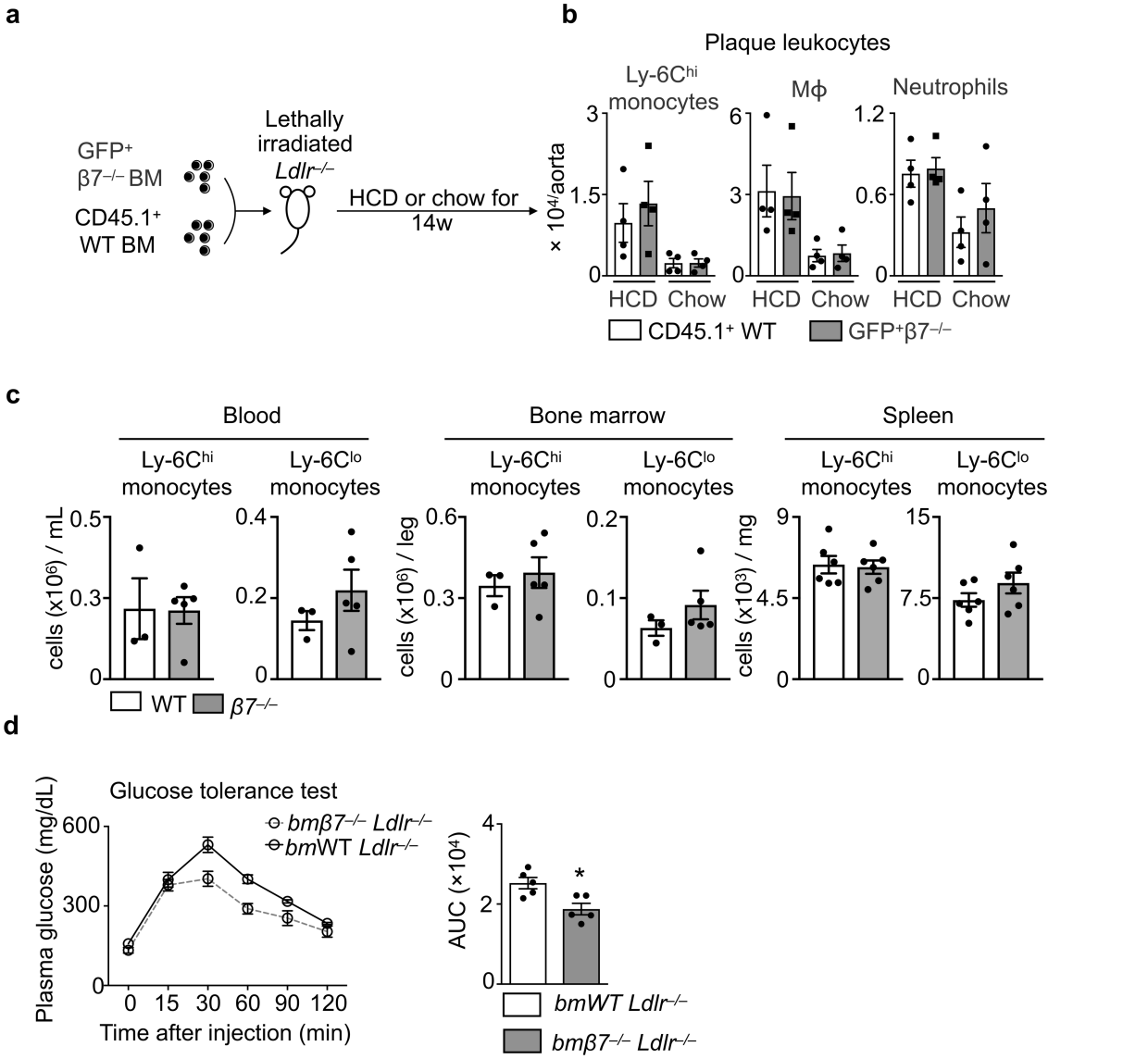

Extended Data Fig. 3 | Effects of integrin β7 deficiency on myeloid cells and glucose tolerance. a, *Ldlr*$^{-/-}$ mice were lethally irradiated and reconstituted with bone marrow mixtures of wild-type and *β7*$^{-/-}$ mice (1:1) and fed a chow diet or HCD for 14 weeks. **b**, The aortic leukocytes from different origins were analysed by flow cytometry. $n = 4$ mice for both HCD recipients and chow recipients. **c**, Ly-6C^{high} and Ly-6C^{low} monocyte numbers in blood ($n = 3$ wild-type mice; $n = 5$ *β7*$^{-/-}$ mice), bone marrow ($n = 3$ wild-type mice; $n = 5$ *β7*$^{-/-}$ mice) and spleen ($n = 6$ mice per group) of wild-type and *β7*$^{-/-}$ mice fed a chow diet. **d**, bm*β7*$^{+/+}$*Ldlr*$^{-/-}$ and bm*β7*$^{-/-}$*Ldlr*$^{-/-}$ mice fed a HCD were subjected to an intraperitoneal glucose-tolerance test. $n = 5$ mice per group; $^{*}P < 0.05$, two-tailed Mann–Whitney *U*-test. Data are mean ± s.e.m.

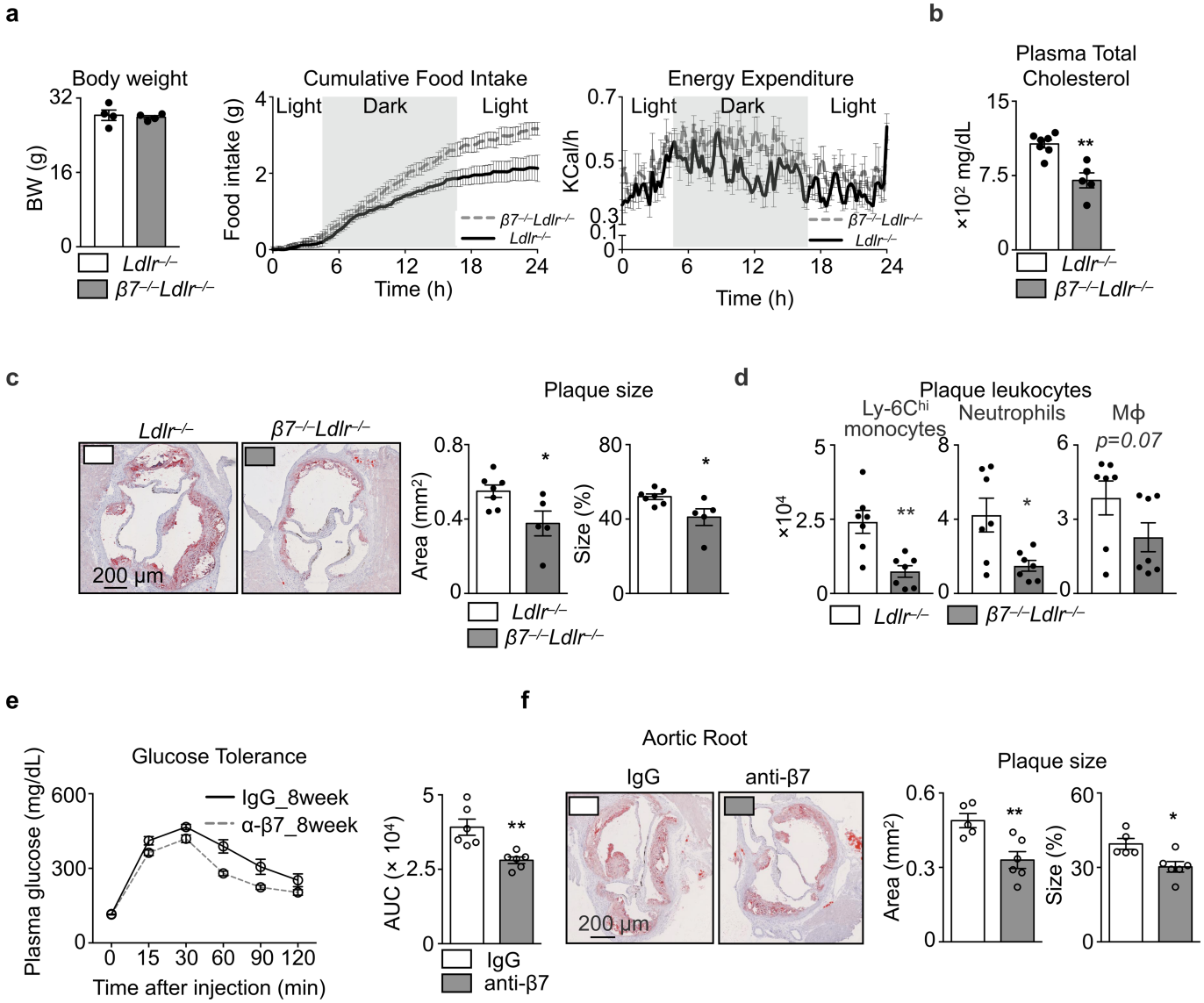

Extended Data Fig. 4 | Effects of genetic deficiency and blocking of integrin β7 on atherosclerosis. a, Body weights, cumulative food intake and energy expenditure were measured in $Ldlr^{-/-}$ mice and $\beta7^{-/-}Ldlr^{-/-}$ mice. $n = 4$ mice per group. **b**, $Ldlr^{-/-}$ mice and $\beta7^{-/-}Ldlr^{-/-}$ mice were fed a HCD for 14 weeks. Plasma cholesterol levels were determined in overnight-fasted mice. $n = 7$ $Ldlr^{-/-}$ mice; $n = 5$ $\beta7^{-/-}Ldlr^{-/-}$ mice; $^{**}P < 0.01$, two-tailed Mann–Whitney *U*-test. **c**, Representative oil-red O images and quantification of plaque size in the aortic roots. $n = 7$ $Ldlr^{-/-}$ mice; $n = 5$ $\beta7^{-/-}Ldlr^{-/-}$ mice; $^{*}P < 0.05$, two-tailed Mann–Whitney *U*-test. **d**, Quantification of Ly-6C^{high} monocytes, neutrophils and macrophages in plaques. $n = 7$ mice per group. $^{*}P < 0.05$, $^{**}P < 0.01$, two-tailed Mann–Whitney *U*-test. **e**, $Ldlr^{-/-}$ mice that were fed a HCD were treated with anti-integrin β7 antibodies or IgG isotype control (500 μg per mouse per week) for 14 weeks. Mice were subjected to a glucose-tolerance test after 8 weeks on the HCD. $n = 6$ mice per group; $^{**}P < 0.01$, two-tailed Mann–Whitney *U*-test. **f**, Representative images of oil-red O-stained aortic cross-sections and quantification of plaque size in the aortic roots after 14 weeks on a HCD. $n = 5$ mice treated with IgG; $n = 6$ mice treated with anti-integrin β7 antibody; $^{*}P < 0.05$, $^{**}P < 0.01$, two-tailed Mann–Whitney *U*-test. Data are mean ± s.e.m.

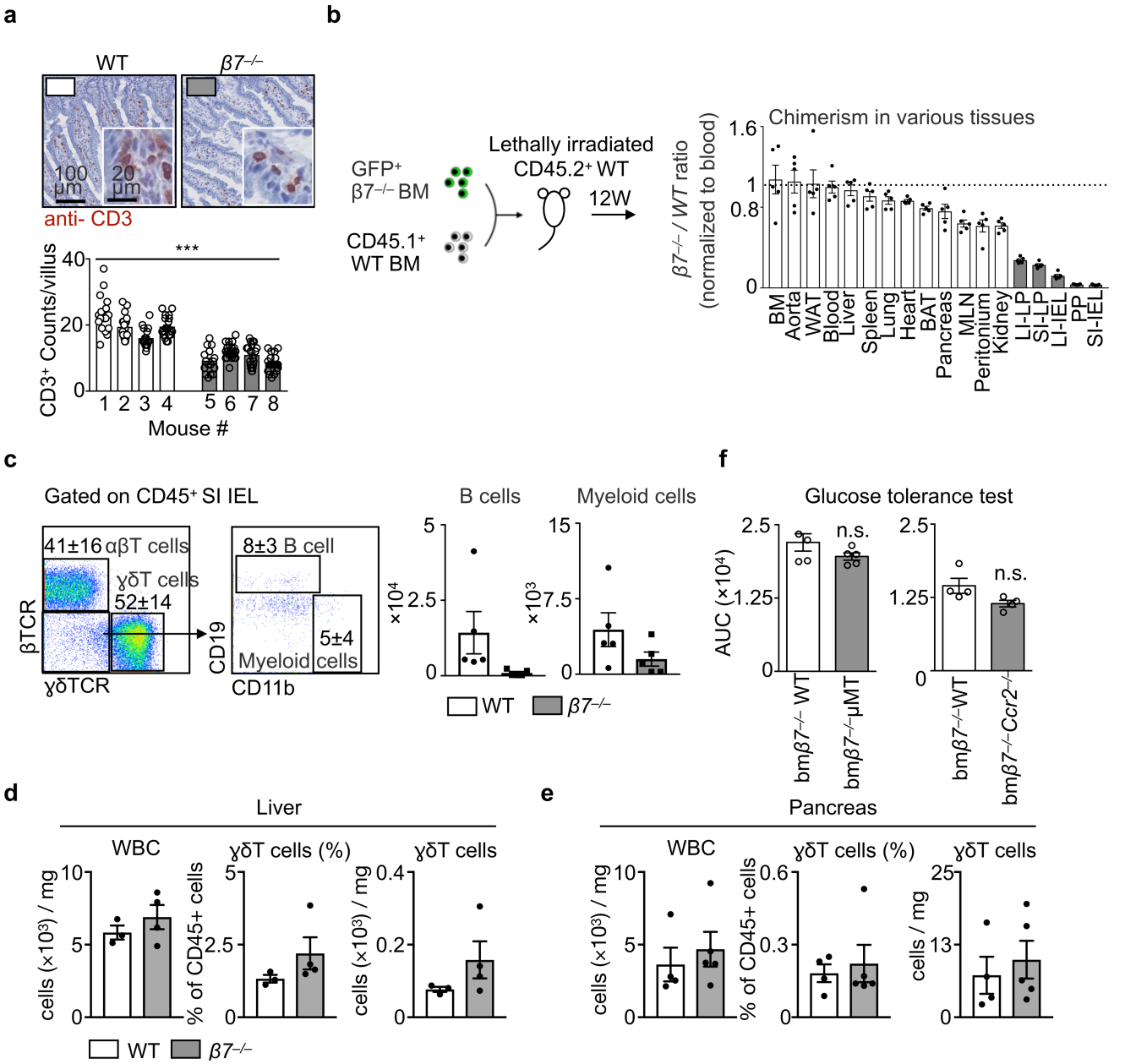

Extended Data Fig. 5 | Integrin β7 guides leukocytes to gut intraepithelium. a, Top, representative histology staining for CD3 in small intestines of wild-type and $\beta7^{-/-}$ mice. Bottom, quantification of $CD3^+$ cells in each villus (more than 15 villi were counted for each mouse). ***$P < 0.001$, two-way ANOVA. **b**, Schematic of the competitive transfer experiments. Mice ($CD45.2^+$) were lethally irradiated and transplanted with a 1:1 ratio mix of $GFP^+\beta7^{-/-}$ bone marrow cells and $CD45.1^+$ wild-type bone marrow cells. The chimerism in different tissues was normalized to the ratio in blood. $n = 5$ mice. **c**, Representative flow cytometry plots and quantification of B cells and myeloid cells in mice depicted in **b**. $n = 5$ biologically independent recipients. **d**, Quantification of γδT cells in the liver. $n = 3$ wild-type mice; $n = 4$ $\beta7^{-/-}$ mice. WBC, white blood cells. **e**, Quantification of γδT cells in the pancreas. $n = 4$ wild-type mice; $n = 5$ $\beta7^{-/-}$ mice. **f**, Wild-type mice were lethally irradiated and reconstituted with bone marrow cell mixtures of $\beta7^{-/-}$ and wild-type ($\beta7^{-/-}$:wild-type cells, 1:1 ratio) or $\beta7^{-/-}$ and indicated knockout mice ($\beta7^{-/-}$:knockout cells, 1:1 ratio). The indicated mixed chimaeras that specifically lack intestinal B cells ($\beta7^{-/-}$μMT) or myeloid cells ($\beta7^{-/-}Ccr2^{-/-}$) were subjected to oral glucose-tolerance tests and the AUCs are shown. $n = 5$ mice per group for $\beta7^{-/-}$ wild-type and $\beta7^{-/-}$μMT mice; $n = 4$ mice per group for $\beta7^{-/-}$ wild-type and $\beta7^{-/-}Ccr2^{-/-}$ mice. Data are mean ± s.e.m.

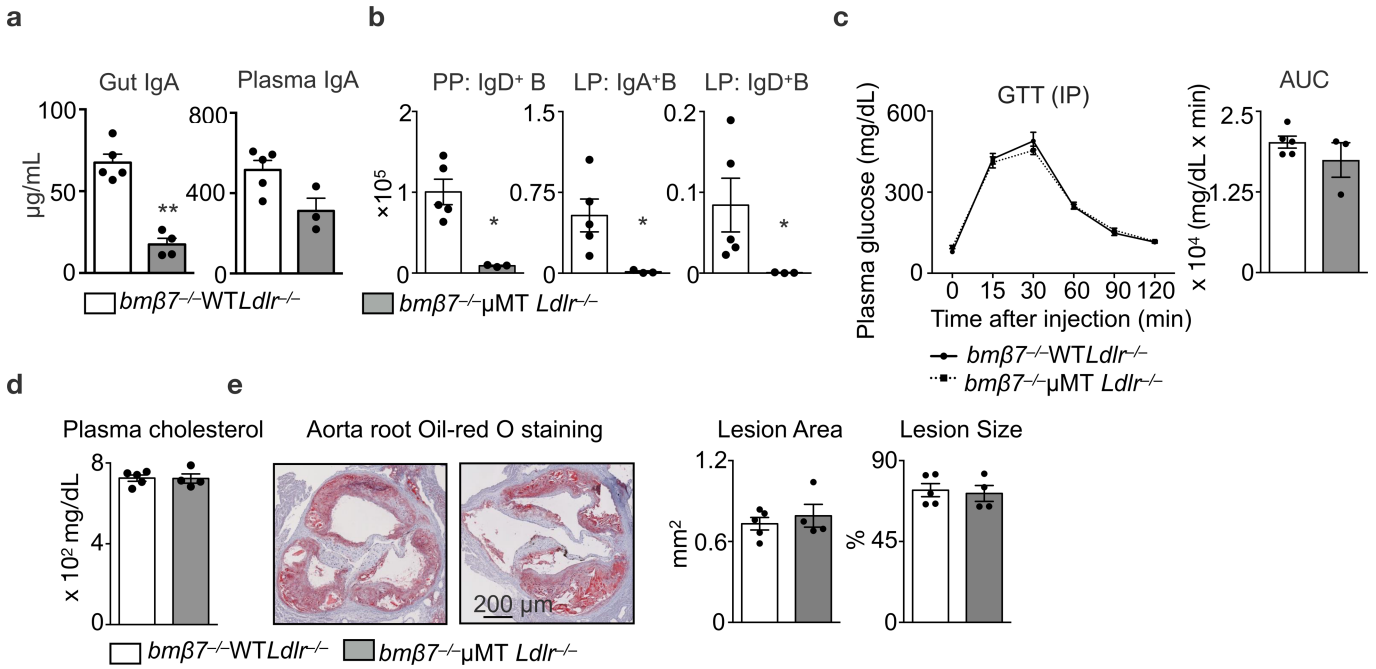

Extended Data Fig. 6 | B cells are dispensable for the altered metabolic phenotypes in integrin β7-deficient mice. *Ldlr*$^{-/-}$ mice were lethally irradiated and reconstituted with bone marrow cell mixtures of *β7*$^{-/-}$ and wild-type (*β7*$^{-/-}$ WT, 1:1 ratio) or *β7*$^{-/-}$ and µMT (*β7*$^{-/-}$µMT, 1:1 ratio). The reconstituted mixed chimaeras were fed a HCD for 14 weeks. **a**, IgA levels in the gut flush ($n = 5$ *β7*$^{-/-}$ wild-type mice; $n = 4$ *β7*$^{-/-}$µMT) and plasma ($n = 5$ *β7*$^{-/-}$ wild-type mice; $n = 3$ *β7*$^{-/-}$µMT mice). $^{**}P < 0.01$, two-tailed Mann–Whitney *U*-test. **b**, Number of IgD$^+$ B cells in Peyer's patches (PP) and IgA$^+$ B cells and IgD$^+$ B cells in lamina propria (LP) as determined by flow cytometry. $n = 5$ *β7*$^{-/-}$ wild-type mice; $n = 3$ *β7*$^{-/-}$µMT mice; $^{*}P < 0.05$, two-tailed Mann–Whitney *U*-test. **c**, Glucose-tolerance test in HCD-fed mixed chimaeras. $n = 5$ *β7*$^{-/-}$ wild-type mice; $n = 3$ *β7*$^{-/-}$µMT mice. **d**, Plasma cholesterol levels in overnight-fasted mice. $n = 5$ *β7*$^{-/-}$ wild-type mice; $n = 4$ *β7*$^{-/-}$µMT mice. **e**, Representative images and quantification of oil-red O staining in aorta root sections of bm*β7*$^{-/-}$ wild-type *Ldlr*$^{-/-}$ mice and bm*β7*$^{-/-}$µMT *Ldlr*$^{-/-}$ mice that were fed a HCD for 14 weeks. $n = 5$ bm*β7*$^{-/-}$ wild-type *Ldlr*$^{-/-}$ mice; $n = 4$ bm*β7*$^{-/-}$µMT *Ldlr*$^{-/-}$ mice. Data are mean ± s.e.m.

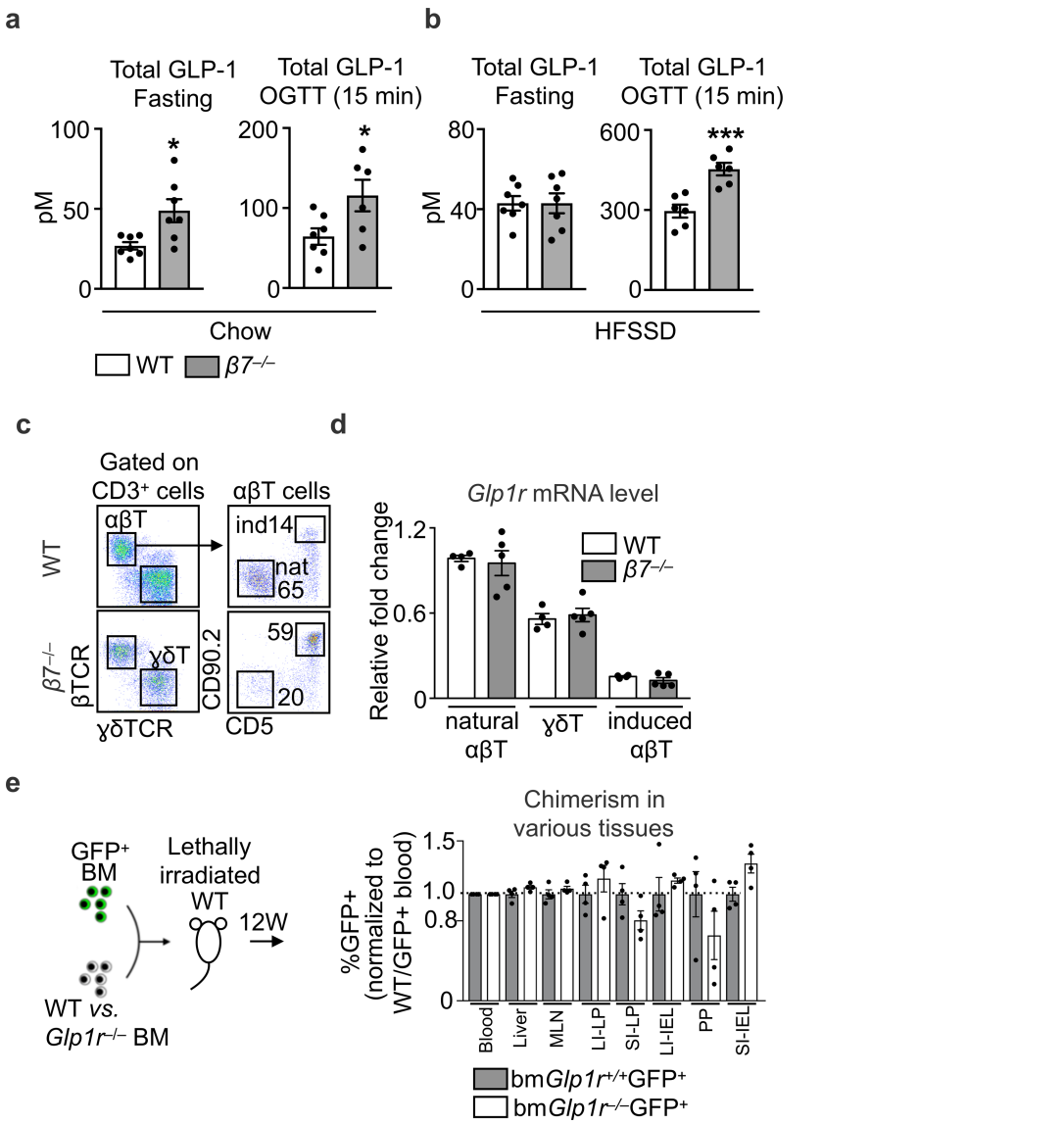

Extended Data Fig. 7 | Integrin β7 deficiency and GLP-1. a, Plasma total GLP-1 levels after overnight fasting and 15 min after oral glucose load (2 g per kg body weight) in wild-type and $\beta7^{-/-}$ mice that were fed a chow diet. Total GLP-1 fasting: $n = 7$ mice per group; total GLP-1 after oral glucose-tolerance test (OGTT) 15 min: $n = 7$ wild-type mice; $n = 6$ $\beta7^{-/-}$ mice. **b**, Plasma total GLP-1 levels after 5 months of a HFSSD. Total GLP-1 fasting: $n = 7$ mice per group; total GLP-1 oral glucose-tolerance test 15 min: 6 mice per group. **c**, Representative flow cytometry plots of small-intestinal IELs from wild-type and $\beta7^{-/-}$ mice. **d**, *Glp1r* mRNA levels in sorted different IEL subsets from wild-type and $\beta7^{-/-}$ mice. $n = 4$ wild-type mice; $n = 5$ $\beta7^{-/-}$ mice. **e**, Wild-type mice were lethally irradiated and transplanted with a 1:1 bone marrow mixture of wild-type and GFP$^+$ or *Glp1r*$^{-/-}$ and GFP$^+$. The chimerism in different tissues was analysed by comparing the percentage of GFP$^+$ leukocytes normalized to wild-type GFP$^+$ blood leukocytes. $n = 4$ mice per group. Data are mean ± s.e.m. $^*P < 0.05$, $^{***}P < 0.001$. All P values from two-tailed unpaired Student's t-tests.

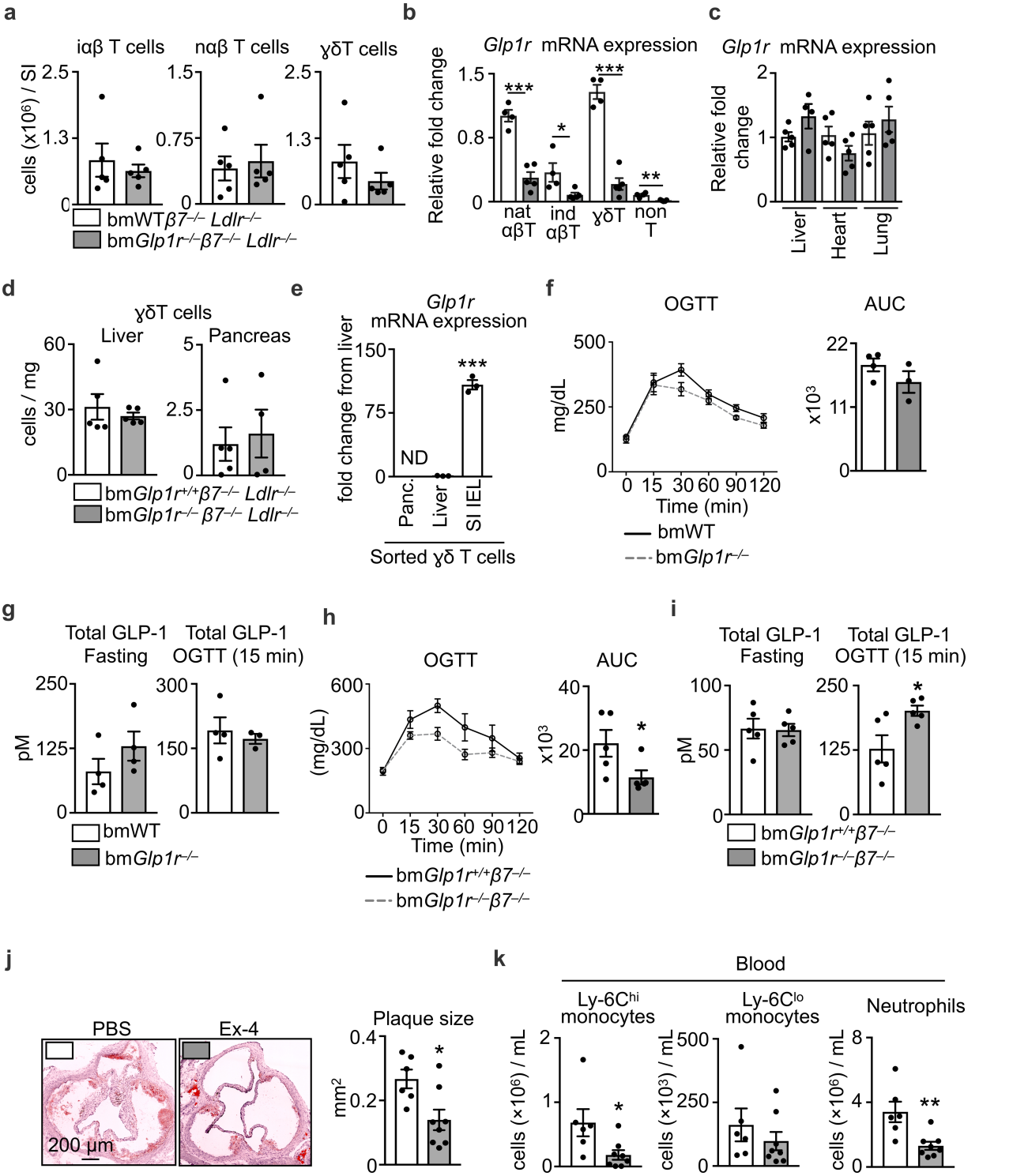

Extended Data Fig. 8 | Effects of Glp1r deficiency on IELs and atherosclerosis. a, Quantification of small-intestinal IEL subpopulations in bm*Glp1r*$^{+/+}$*β7*$^{-/-}$*Ldlr*$^{-/-}$ and bm*Glp1r*$^{-/-}$/*β7*$^{-/-}$*Ldlr*$^{-/-}$ mice. $n = 5$ mice per group, mean ± s.e.m. **b**, *Glp1r* mRNA expression of sorted IEL subpopulations. $n = 4$ biologically independent bm*Glp1r*$^{+/+}$*β7*$^{-/-}$ and $n = 5$ biologically independent bm*Glp1r*$^{-/-}$*β7*$^{-/-}$ mice; two-tailed unpaired Student's *t*-test. **c**, *Glp1r* mRNA expression in the liver ($n = 5$ bm*Glp1r*$^{+/+}$*β7*$^{-/-}$ and $n = 4$ bm*Glp1r*$^{-/-}$*β7*$^{-/-}$ mice), heart and lung tissue ($n = 5$ mice per group). **d**, Quantification of γδ T cells from the liver ($n = 5$ mice per group) and pancreas ($n = 5$ bm*Glp1r*$^{+/+}$*β7*$^{-/-}$*Ldlr*$^{-/-}$ mice; $n = 4$ bm*Glp1r*$^{-/-}$*β7*$^{-/-}$*Ldlr*$^{-/-}$ mice). **e**, *Glp1r* mRNA expression of sorted γδ T cells from pancreas, liver and small-intestinal IELs. $n = 3$ mice per group; two-tailed unpaired Student's *t*-test. **f**, Oral glucose-tolerance test. $n = 4$ bm*Glp1r*$^{+/+}$ mice; $n = 3$ bm*Glp1r*$^{-/-}$ mice. **g**, GLP-1 levels after overnight fasting ($n = 4$ mice per group) or oral glucose challenge ($n = 4$ bm*Glp1r*$^{+/+}$ mice; $n = 3$ bm*Glp1r*$^{-/-}$ mice). **h**, Oral glucose-tolerance test in bm*Glp1r*$^{+/+}$*β7*$^{-/-}$ and bm*Glp1r*$^{-/-}$*β7*$^{-/-}$ mice. $n = 5$ mice per group; two-tailed Mann–Whitney *U*-test. **i**, GLP-1 levels after overnight fasting or oral glucose challenge in bm*Glp1r*$^{+/+}$*β7*$^{-/-}$ and bm*Glp1r*$^{-/-}$*β7*$^{-/-}$ mice. $n = 5$ mice per group; two-tailed unpaired Student's *t*-test. **j**, *Ldlr*$^{-/-}$ mice were treated with the GLP-1 receptor agonist exendin-4 (Ex-4) at a dose of 100 μg per kg per day via osmotic minipumps (PBS was used as control). After 8 weeks on a HCD, mice were euthanized to enable the quantification of atherosclerotic lesions. Representative images of oil-red O-stained aortas and quantification of plaque size. **k**, Quantification of blood Ly-6C^{high} monocytes, Ly-6C^{low} monocytes and neutrophils. $n = 8$ *Ldlr*$^{-/-}$ mice treated with exendin-4; $n = 6$ *Ldlr*$^{-/-}$ mice treated with PBS; two-tailed unpaired Student's *t*-test. Data are mean ± s.e.m. $^{*}P < 0.05$, $^{**}P < 0.01$, $^{***}P < 0.001$.

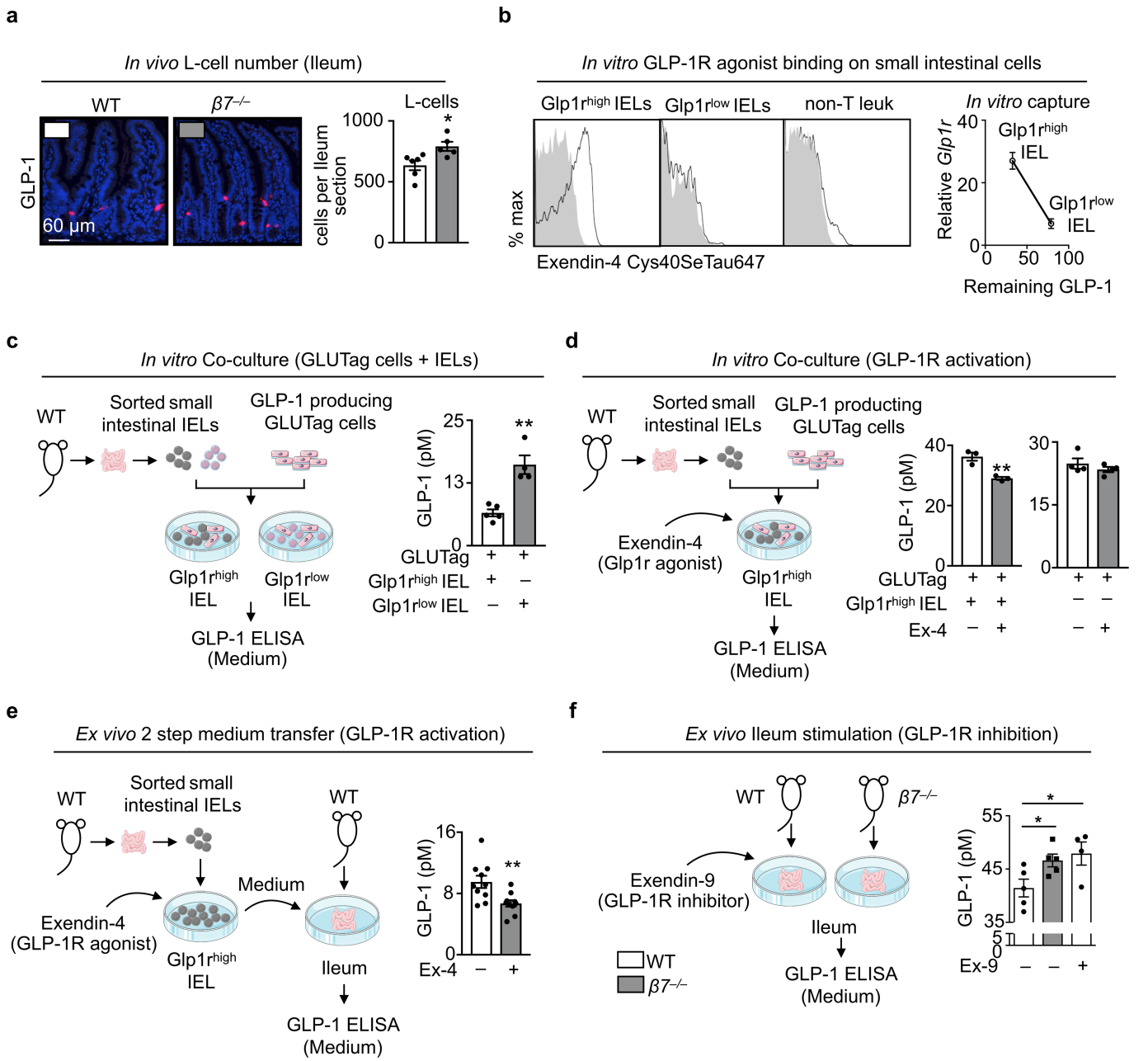

Extended Data Fig. 9 | Gut intraepithelial Glp1r^{high} IELs regulate the bioavailability of GLP-1. a, Immunohistochemistry and quantification of GLP-1-producing L-cells in whole ileum preparations of 6 wild-type and 5 $\beta7^{-/-}$ mice. **b**, Small-intestinal IEL mixtures were incubated with the fluorescently (Cys40SeTau647) labelled GLP-1R agonist exendin-4 and the capacity of agonist binding by the different subsets—natural IELs (Glp1r^{high}), induced IELs (Glp1r^{low}) and non-T cells—was analysed by flow cytometry. Sorted Glp1r^{high} and Glp1r^{low} cells were also incubated with recombinant GLP-1 and the remaining supernatant GLP-1 was plotted against the relative *Glp1r* mRNA levels of the cells. **c**, GLP-1-producing GLUTag cells were co-cultured with sorted natural (Glp1r^{high}) or induced (Glp1r^{low}) IELs. After 24 h, the concentration of GLP-1 in the supernatant was measured. $n = 5$ biologically independent samples for Glp1r^{high} IELs and $n = 4$ biologically independent samples for Glp1r^{low} IELs. **d**, Left, GLUTag cells were co-cultured with sorted Glp1r^{high} IELs in the presence of exendin-4 (100 nM) or control. $n = 3$ independent biologically samples per group. Right, GLUTag cells were stimulated with exendin-4 (100 nM) or control. $n = 4$ independent biological samples per group. After 24 h, the concentration of GLP-1 in the supernatant was measured. **e**, Sorted Glp1r^{high} IELs were incubated with exendin-4 (100 nM) or control. After 24 h, samples were centrifuged and supernatants were transferred to ex vivo ileum fractions of wild-type mice. GLP-1 levels were determined 24 h later from ex vivo supernatants. $n = 10$ biologically independent mice per group. **f**, Whole gut preparations of wild-type or $\beta7^{-/-}$ mice were treated with or without the GLP-1 receptor antagonist exendin-9 (100 nM). After 24 h, the concentration of GLP-1 in the supernatant was measured. $n = 5$ biologically independent samples for wild-type or $\beta7^{-/-}$ mice without exendin-9; $n = 4$ biologically independent samples for wild-type mice with exendin-9. Data are mean ± s.e.m. $^*P < 0.05$, $^{**}P < 0.01$. All P values from two-tailed unpaired Student's t-test.

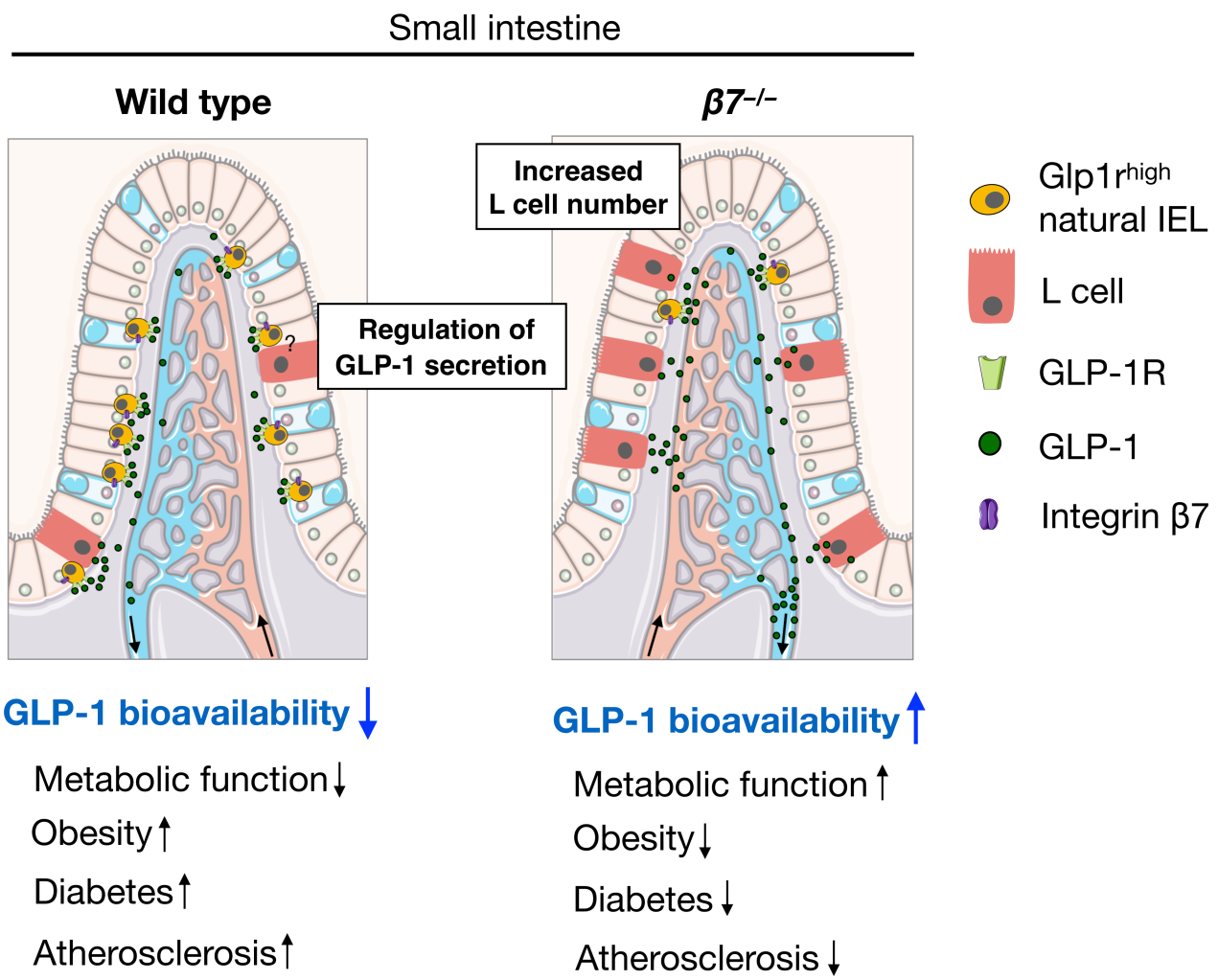

Extended Data Fig. 10 | Model. In this study, we propose that integrin β7-dependent Glp1r^{high} IELs that reside in the small intestine modulate dietary metabolism in mice by restricting the bioavailability of GLP-1.

The illustration was modified from Servier Medical Art (http://smart.servier.com/), licensed under a Creative Common Attribution 3.0 Generic License.

nature research

Corresponding author(s): Filip Swirski; Shun He

Reporting Summary

Nature Research wishes to improve the reproducibility of the work that we publish. This form provides structure for consistency and transparency in reporting. For further information on Nature Research policies, see Authors & Referees and the Editorial Policy Checklist.

Statistical parameters

When statistical analyses are reported, confirm that the following items are present in the relevant location (e.g. figure legend, table legend, main text, or Methods section).

n/a	Confirmed	
☐	☒	The exact sample size (*n*) for each experimental group/condition, given as a discrete number and unit of measurement
☐	☒	An indication of whether measurements were taken from distinct samples or whether the same sample was measured repeatedly
☐	☒	The statistical test(s) used AND whether they are one- or two-sided *Only common tests should be described solely by name; describe more complex techniques in the Methods section.*
☐	☒	A description of all covariates tested
☐	☒	A description of any assumptions or corrections, such as tests of normality and adjustment for multiple comparisons
☐	☒	A full description of the statistics including central tendency (e.g. means) or other basic estimates (e.g. regression coefficient) AND variation (e.g. standard deviation) or associated estimates of uncertainty (e.g. confidence intervals)
☐	☒	For null hypothesis testing, the test statistic (e.g. *F*, *t*, *r*) with confidence intervals, effect sizes, degrees of freedom and *P* value noted *Give P values as exact values whenever suitable.*
☒	☐	For Bayesian analysis, information on the choice of priors and Markov chain Monte Carlo settings
☒	☐	For hierarchical and complex designs, identification of the appropriate level for tests and full reporting of outcomes
☒	☐	Estimates of effect sizes (e.g. Cohen's *d*, Pearson's *r*), indicating how they were calculated
☐	☒	Clearly defined error bars *State explicitly what error bars represent (e.g. SD, SE, CI)*

Our web collection on statistics for biologists may be useful.

Software and code

Policy information about availability of computer code

Data collection	BD FACSDiVa™ software was used to collect data from flow cytometry; NPDview2 software, NanoZoomer 2.0RS software and NIH ImageJ program were used to collect immunohistochemistry data; Columbus CLAX 2.2.10 was used to collect data for metabolic measurements; Thermo Scientific™ Amira™ Software 5.3.2 was used for 18-FDG-PET/CT imaging.
Data analysis	Flow cytometric analyses were performed with the FlowJo analysis software (FlowJo 8.7.2); Statistical analyses were performed with the GraphPad Prism 7.0 software (GraphPad)

For manuscripts utilizing custom algorithms or software that are central to the research but not yet described in published literature, software must be made available to editors/reviewers upon request. We strongly encourage code deposition in a community repository (e.g. GitHub). See the Nature Research guidelines for submitting code & software for further information.

Data

Policy information about availability of data

All manuscripts must include a data availability statement. This statement should provide the following information, where applicable:

- Accession codes, unique identifiers, or web links for publicly available datasets
- A list of figures that have associated raw data
- A description of any restrictions on data availability

The authors declare that the data supporting the findings of this study are available within the paper [and its supplementary information files].

Field-specific reporting

Please select the best fit for your research. If you are not sure, read the appropriate sections before making your selection.

☒ Life sciences ☐ Behavioural & social sciences ☐ Ecological, evolutionary & environmental sciences

For a reference copy of the document with all sections, see nature.com/authors/policies/ReportingSummary-flat.pdf

Life sciences study design

All studies must disclose on these points even when the disclosure is negative.

Sample size	Sample size calculations were carried out using group percentages (controls expressing 90% expected value) and variables expressing 20-30% change, which was deemed to be detectable changes using our current imaging and ex vivo analytical methods. Confidence levels were set at 5% with Beta levels established as 50%.
Data exclusions	No data was excluded from the analysis
Replication	All attempts at replication were successful. Findings were replicated in at least three biologically independent samples each.
Randomization	Allocation of animals (mice) into different experimental groups was done in a random manner
Blinding	Investigators were blinded to group allocation during data collection and analysis

Reporting for specific materials, systems and methods

Materials & experimental systems

n/a	Involved in the study
☒	☐ Unique biological materials
☐	☒ Antibodies
☐	☒ Eukaryotic cell lines
☒	☐ Palaeontology
☐	☒ Animals and other organisms
☒	☐ Human research participants

Methods

n/a	Involved in the study
☒	☐ ChIP-seq
☐	☒ Flow cytometry
☒	☐ MRI-based neuroimaging

Antibodies

Antibodies used

anti-integrin β7 (BioLegend, clone FIB27, Cat#121008, Lot#B238485), anti-CD45 (BioLegend, Clone30-F11, Cat#103147, Lot#B243834), anti-CD45.1 (BioLegend, clone A20, Cat#110708), anti-CD45.2 (BioLegend, clone 104, Cat#109802), anti-CD3 (BioLegend, clone 17A2, Cat#100206), anti-CD90.2 (BioLegend, clone 30-H12, Cat#105308, Lot#B237375), anti-CD19 (BioLegend, clone 6D5, Cat#115508, Lot#B226581), anti-B220 (BD Biosciences, clone RA3-6B2, Cat#553089, Lot#6012954), anti-NK1.1 (BioLegend, clone PK136, Cat#108708), anti-Ly-6G (BioLegend, clone 1A8, Cat127614#, Lot#B259670), anti-Ly-6C (BioLegend, AL-21, Cat#128006, Lot#B247728), anti-MHCII (BioLegend, clone M5/114.152, Cat#107602, Lot#B217859), anti-F4/80 (Biolegend, clone BM8, Cat#123114, Lot#B237342) anti-CD11b (BioLegend, clone M1/70, Cat#101226, Lot#B238268), anti-CD5 (BioLegend, clone 53-7.3, Cat#100618, Lot#B208112), anti-βTCR (BioLegend, clone H57-597, Cat#109206, Lot#B202917), anti-γ/δTCR (BioLegend, clone GL3, Cat#118116, Lot#B228498), anti-CD326 (BioLegend, clone G8.8, Cat#118214), anti-IgA (BD Biosciences, clone C10-3, Cat#559354, Lot#5089919), anti-IgD (BioLegend, clone 11-26c.2a, Cat#405725, Lot#B219485), anti-CD115 (BioLegend, clone AFS98, Cat#135517, Lot#B265220), anti-CX3CR1 (BioLegend, clone SA011F11, Cat#149027, Lot#B247422), anti-CD90.2 (BD Pharmingen, clone 53-2.1, Cat#561642, Lot#8145588), anti-CD5 (BD Horizon, clone 53-7.3,

	Cat#563194, Lot#7355892), anti-CD19 (BioLegend, clone 6D5, Cat#115540, Lot#B216486), anti-CD3 (BioLegend, clone 17A2, Cat#100204, lot#B184713), anti-Ly-6C (BioLegend, clone HK1.4, Cat#128036, Lot#B245767), anti-CD19 (BioLegend, clone 6D5, Cat#115530, Lot#B228154), anti-CD5 (BioLegend, clone 53-7.3, Cat#100623, Lot#B200347). All antibodies were used in a 1:700 dilution.
Validation	These antibodies are all used for flow cytometry for experiments with mice. Antibody validations were performed by antibody suppliers per quality assurance literature provided by each supplier.

Eukaryotic cell lines

Policy information about cell lines

Cell line source(s)	GLUTag cells were kindly provided by Dr. Daniel J. Drucker (Lunenfeld-Tanenbaum Research Institute, Mount Sinai Hospital, Joseph & Wolf Lebovic Health Complex, Toronto, ON, Canada.
Authentication	The GLUTag cell line was isolated from a glucagon-producing enteroendocrine cell tumor that arose in glucagon gene-SV40 T antigen transgenic mice. The cell line was generated, first described and authenticated by Dr. Daniel J. Drucker (Drucker et al. Mol Endocrinol. 1994; Brubaker et al. Endocrinology. 1998). The GLUTag cell line has been repeatedly authenticated by many different international laboratories by validating secretion of enteroendocrine hormones (i.e. GLP-1, GLP-2) and the typical gene expression profile. The respective references can be found at http://glucagon.com/glutagcells.html.
Mycoplasma contamination	The GLUTag cell line has been tested negative for mycoplasma contamination
Commonly misidentified lines (See ICLAC register)	GLUTag cells are not listed in the database of commonly misidentified cell lines

Animals and other organisms

Policy information about studies involving animals; ARRIVE guidelines recommended for reporting animal research

Laboratory animals	C57BL/6J (wild type, WT), Itgb7tm1Cgn (β7–/–), Ldlrtm1Her (Ldlr–/–), Tcrbtm1Mom (βTCR–/–), Tcrdtm1Mom (γδTCR–/–), Ccr2tm1Ifc (Ccr2–/–), Ighmtm1Cgn (μMt), Ccr9tm1Lov (Ccr9–/–), Itgaetm1Cmp (itgae–/–) mice either male or female were purchased from The Jackson Laboratory (Bar Harbor, ME, USA). Glp1r–/– male mice in the C57BL/6 background were bred in-house as described. Unless otherwise indicated age- and sex-matched animals were used at 8–12 weeks of age. Where appropriate, animals were randomly assigned to interventions.
Wild animals	This study did not involve wild animals
Field-collected samples	This study did not involve samples collected from the field

Flow Cytometry

Plots

Confirm that:

☐ The axis labels state the marker and fluorochrome used (e.g. CD4-FITC).

☐ The axis scales are clearly visible. Include numbers along axes only for bottom left plot of group (a 'group' is an analysis of identical markers).

☒ All plots are contour plots with outliers or pseudocolor plots.

☒ A numerical value for number of cells or percentage (with statistics) is provided.

Methodology

Sample preparation	Peripheral blood was collected by retro-orbital bleeding and red blood cells were lysed in RBC lysis buffer (BioLegend, San Diego, CA). Aortas were excised after PBS (Thermo Fisher Scientific, MA) perfusion, minced and digested with 450 U/ml collagenase I, 125 U/ml collagenase XI, 60 U/ml DNase I and 60 U/ml hyaluronidase (Sigma-Aldrich, St. Louis, MO) in PBS for 40 minutes at 37℃. Total viable cell numbers were counted using trypan blue (Cellgro, Mediatech, Inc. VA). Small intestine intraepithelial leukocytes (IEL) were isolated as follows: After excision of the small intestine, the Peyer's patches were removed under microscope and the gut was cut open longitudinally to wash off the lumen contents in HBSS buffer. The gut was then cut into 1-2 cm pieces and subjected to 3 x dissociation in EDTA-containing buffer (7.5 mM HEPES, 2% FCS, 2 mM EDTA, 10.000 U/mL Penicillin-Streptomycin, 50 μg/mL Gentamycin in HBSS; all Thermo Fisher Scientific, MA) in a shaker at 37℃ for 15 minutes. After dissociation the IELs were collected by filtering lamina propria through a mesh. For sorting, the IEL flow-through after dissociation was further subjected to Percoll (GE Healthcare Bio-Sciences, MA) gradient centrifugation to remove the mucus. Single cell suspension of IELs from indicated animals were then stained to identify indicated cell populations.
Instrument	FACS LSRII, FACS Aria II
Software	DIVA, FlowJo
Cell population abundance	After sorting, a small fraction of the sorted cells were run through Aria II and the same gating strategy was applied to check the

Cell population abundance	purity of sorted cell populations. A general purity of higher than 95% were achieved for all the sorted population.
Gating strategy	For Fig S2a,b, the gating strategy is: FSC-A/SSC-A (cells)--- FSC-A/FSC-H (singlets)--- CD45-BV711/SSC-A (leukocytes) --- CD45-BV711/ Zombie-BV510 (live leukocytes) --CD19-BV605/CD3-FITC (Non TB leukocytes). For Fig 3, Fig S3a,b,c, S4, S8k and Fig 4, the gating strategy is: FSC-A/SSC-A (cells)--- FSC-A/FSC-H (singlets)--- CD45-BV711/SSC-A (leukocytes) --- CD45-BV711/ Zombie-BV510 (live leukocytes)--- Lin-PE/CD11b-APCCy7 (myeloid cells)--- Ly6C-BV605 or FITC/F4/80- PECy7 (Ly-6Chi monocytes, Ly-6Clo monocytes, neutrophils, macrophages). For Fig S5, the gating strategy is: FSC-A/SSC-A (cells)--- FSC-A/FSC-H (singlets)--- CD45-BV711/SSC-A (leukocytes) --- CD45-BV711/ Zombie-BV510 (live leukocytes). For Fig S6, the gating strategy is: FSC-A/SSC-A (cells)--- FSC-A/FSC-H (singlets)--- CD45-BV711/SSC-A (leukocytes) --- CD45-BV711/ Zombie-BV510 (live leukocytes)-- CD3-PE/CD19-APCCy7(B cells)-- CD3-PE/IgD-BV421 or IgA-FITC (IgD+ or IgA+ B cells). For Fig S7c, S8 a,d, the gating strategy is: FSC-A/SSC-A (cells)--- FSC-A/FSC-H (singlets)--- CD45-BV711/SSC-A (leukocytes) --- CD45-BV711/ Zombie-BV510 (live leukocytes)-- CD3-PE/CD19-APCCy7--- bTCR-FITC/gdTCR-APC (abT, gdT cells) ---- CD90.2-PECy7/CD5-PerCPCy5.5 or BV605 (natural abT or nabT, induced abT or iabT)

☒ Tick this box to confirm that a figure exemplifying the gating strategy is provided in the Supplementary Information.